Sunspot analysis under varying conditions climate: Distributed radiation on cooling floor and its effect on dynamic thermal behaviour

M.H. Benzaama, A.M. Mokhtari, Mohammed Lachi, Chadi Maalouf, S. Menhoudj

Sunspot analysis under varying conditions climate: distributed radiation on cooling floor and its effect on dynamic thermal behaviour

M. H. Benzaama [a], A.M. Mokhtari [b], M. Lachi [c], C. Maalouf [c], S. Menhoudj [b]

[a] COMUE Normandie Université - Laboratoire de Recherche ESITC - ESITC Caen, 1 Rue Pierre et Marie Curie 14610 Epron, France

[b] LMST Laboratory, University of Sciences and Technology, Mohamed BOUDIAF, Oran, Algeria

[c] MATIM Laboratory, Université de Reims Champagne Ardenne, Reims, France

Abstract

The dynamic thermal simulation of buildings is a real challenge, in terms of regulations and labelling but also of decisions (implementation, materials choice, architectural design, rehabilitation ...). Today, we lack reference models of the dynamic thermal behaviour of the cooling floor under solar radiation effect. In fact, the simulation models developed in literature are represented in a very simplified method and cannot be used for a detailed analysis of thermal comfort. The present study aims to reduce the knowledge gap and resolve the limitations such as (i) studying the effect of sunspot for a real weather conditions, (ii) visualize the dynamic thermal behaviour of indoor air and surface cooling floor relative to the sunspot shifting and (iii) predict different sunspot shape as a function of geographic location. A 3D model is presented in this paper to evaluate the sunspot impact on cooling floor coupled to underground tank under climatic conditions in Algeria. The sunspot is calculated using a coupled TRNSYS-FLUENT dynamic simulation. Simulations are run for different periods and weather conditions. The results have shown that the developed model can provide a real simulation of thermal performance of the cooling floor taking into account the sunspot shifting. The incident solar heat flux on cooling floor reaches a maximum of 300 W/m^2 for Bechar city and 120 W/m^2 for Oran city. A wide surface temperature ranges of 13°C between the umbrageous and illuminated areas. For Oran weather conditions, the indoor air temperature in the

umbrageous area is around 24 °C, while that of the illuminated area is 28 °C which can cause a temperature heterogeneity in the room.

Key words: Cooling floor, sunspot, dynamic thermal behaviour, coupling TRNSYS-FLUENT.

Nomenclature

Roman and greek letter symbols

$\boldsymbol{T}$	temperature (°C)
$\boldsymbol{\rho}$	density (kg/m^3)
$\boldsymbol{C_p}$	heat capacity of water (J/kg.K)
$\boldsymbol{\dot{m}}$	mass flow rate (kg/s)
$\boldsymbol{\alpha_{soil}}$	soil thermal diffusivity (m^2/s)
$\boldsymbol{A_s}$	amplitude of soil surface temperature throughout the year (K)
$\boldsymbol{T_m}$	mean surface temperature (°C)
$\boldsymbol{t}$	time (hour)
$\boldsymbol{t_0}$	time of year with minimum soil surface temperature (hour)
$\boldsymbol{Z}$	soil depth (m)
$\boldsymbol{UA}$	overall loss coefficient (W/K)

$\boldsymbol{h}$	convective heat transfer coefficient ($W/m^2.K$)
$\Delta \boldsymbol{T_{ln}}$	logarithmic temperature (°C)
$\Delta \boldsymbol{h}$	separation between centers of segments
g	Gravitational acceleration (m/s^2)
β	Thermal expansion coefficient
ρ_0	Fluid density at T0 (kg/m^3)
A	Apparent solar radiation at air mass m = 0
B	Atmospheric extinction coefficient
β	Solar altitude
S_{etrn}	The top of the atmosphere direct normal solar irradiance.
E_{dn}	Direct normal irradiation at the earth's surface on a clear day
ε	Tilt angle of the surface from the horizontal plane
ρ_g	Ground reflectivity

Subscripts

s	Soil
surf	surface
w	water
in	Inlet
Out	Outlet
UNT	Underground tank

1. Introduction

The reduction of fossil-based energy use continues to be the primary concern in all areas of research. For high-performance buildings, low-temperature heating is one of the practical solutions to reduce energy use and cooling energy needs. For this purpose, and in order to reduce the considerable building sector's energy consumption, Algeria is initiating a green energy dynamic by launching an ambitious development of renewable energies and energy efficiency program [1]. In this context, several renewable energy technologies for cooling can be considered, one such approach is the geothermal systems. These systems are used to transfer thermal energy stored in the ground, with the aim of reducing the energy demand of buildings' cooling. Two different types of geothermal systems for cooling are used in the Algerian context: blowing fresh air and cooling floor coupled to the geothermal systems. Several studies have been made for the Algerian climate on geothermal cooling systems by blowing fresh air (air earth-to-air heat exchangers) such as Nasreddine Sakhri et al., [2-10]. Furthermore, M. H. Benzaama el al., [11, 12] have studied the energy efficiency of seasonal storage coupled with a cooling floor. The studies were devoted solely to the efficiency of the geothermal system, without a thorough analysis of the cooling floor.

A cooling floor system presents the potential to improve the indoor thermal comfort and provides optimal heat distribution in the occupied area. In cooling, several studies indicate two major problems. The first is the risk of condensation and the second is overheating. For the condensation problem, the temperature of the cooling floor surface must be higher than dew temperature. In this purpose, several researchers have been interested in modelling the surface temperature of a cooling floor such as Xiaozhou Wu et al., [13]. A parametric study was carried out on the influence of the average water temperature, the spacing step and the thickness of each layer of the cooling floor on the surface temperature. The results show that to decrease the surface temperature, the spacing step and the average water temperature must be reduced. Furthermore, Lun Zhang et al., [14] have shown that the thickness of each layer of the cooling floor has no effect on the surface temperature and heat transfer. Moreover, Xing Jin et al. [15] have shown that a thermal conductivity of the hydraulic circuit has an effect on the performance of the cooling floor. However, the effect of water speed does not have a significant effect on the cooling system.

Cooling floor Overheating due to solar gains have been the subject of several studies focusing on analyzing their effect on thermal comfort. K. Zhao et al., [16] studied the effect of solar radiation on the cooling capacity of the cooling floor. A calculation method has been proposed to study the effect of the different emissivity values of the wall surface on the cooling capacity. They reported that the cooling capacity of the cooling floor increased significantly when exposed to a solar beam of 40–100 Wm^{-2}.

Tian et al., [17] et Feng et al., [18] have established a new model to calculate the cooling capacity as a function of solar radiation transmitted by the window. However, the models developed impose that the heat solar flux is uniform on cooling floor. Moreover, Michel de carli et al., [19] have shown that we can't have a precise simulations using a simplified model. In this context, there are several simplified models in literature for the study of solar radiation effect on cooling floor such as RC-network model, software simulation programs as TRNSYS and heat conduction transfer function. However, for real conditions, solar heat flux is only received on part of the cooling floor called sunspot. Some studies have been conducted concerning the sunspot simulation such as K. Kontoleon [20]. As drawbacks, the proposed

model does not allow to evaluate the dynamic thermal behaviour of indoor air depending on the sunspot localization. Furthermore, for Tunisian climate conditions, Boukhris et al., [21] proposed for a passive building, a sunspot calculation method using ZAER tool. The inconvenience of this method that is able to evaluate only parallelepiped-shape rooms due to the rectangular characteristic of the mesh.

For Algerian climate conditions, S. Saadi et al., [22] developed a thermal models taking into consideration the sunspot area on the internal walls. This model can't predict the real location of the sunspot on the floor for example. Nevertheless, we can't visualize in 3D, the sunspot movement and the dynamic thermal behavior of the indoor air relative to the sunspot localization.

An experimental study was made by C. Beji, et al., [23] on the effect of the sunspot on the heating floor. As drawbacks, the solar patch was experimentally simulated by an electric heating film with a modulated power. The solar intensity was kept constant with a rectangular constant shape

The study of the effect of the sunspot was made on passive buildings and buildings equipped with a heating floor. To our best knowledge, there is just one research on the effect of the sunspot on the cooling floor. Haida Tang et al., [24] developed a 3D model to simulate the sunspot thermal behaviour on cooling floor. The authors found the difficulty to track the localization and the movement of the sunspot. In addition, indoor air temperature is assumed uniform despite the existence of the sunspot, and the distribution of entering solar heat flux on the floor was imposed. On other hand, few researchers took an interest in the absorbed solar heat flux. Athienitis and Stylianou [25] and Cucumo et al [26], showed an approach to evaluate the solar absorbance of a room, based on the radio-irradiation method (RIM) algorithm developed by Sparrow and Cess [27]. Absorbed solar radiation is presented in relation to the number of elements that the surface of the wall is divided. For the sunspot models presented in the literature, the solar power absorbed and reflected at the sunspot location has not been developed.

In the present study, the effect of sunspot on the thermal behaviour of a cooling floor coupled with a geothermal system is presented. According to the state of the art, the sunspot effect has been addressed

by few researchers. Just one study has been devoted to the effect of sunspot on cooling floor [24]. Moreover, the published numerical sunspot models do not represent the reality. This models don't provide a realistic explanation of the thermal behaviour of cooling floor. Several limitations can be summarized under the following issues:

1. The solar power received on the cooling floor is imposed. The real climatic conditions are not taken into account;
2. Real-time sunspot tracking is not detailed;
3. The heat flux emitted by the sunspot has never evaluated;
4. The 3D visualization of the whole room influenced by the sunspot at different time and climate conditions is not presented
5. The dynamic thermal behaviour of indoor air is considered uniform even with the presence of sunspot.

The limitations mentioned above indicate a knowledge deficit that needs to be addressed. Without addressing these limitations, we will not be able to provide accurate cooling floor sizing for different climates. The present study aims to reduce this knowledge gap and resolve the limitations such as (i) studying the effect of sunspot for a real weather conditions, (ii) visualize the dynamic thermal behaviour of indoor air and surface cooling floor relative to the sunspot shifting and (iii) predict different sunspot shape related to the geographic location. For this purpose, a methodology has been developed by combining the two software programs TRNSYS and FLUENT. This method allows to model the cooling floor of an experimental cell coupled with a seasonal storage system by TRNSYS tools and combined it with the sunspot model developed on FLUENT. It should be noted that the developed model was performed for two different climate types in Algeria including 1) Oran with Mediterranean climate and 2) Bechar with Arid climate.

116 The paper is organized as follows: Section 2 describes the methodology of the study. Then, the
117 experimental device and the numerical model are presented in section 3 and 4. The sections 5, 6, and 7
118 are dedicated to the analysis of the results and their discussion, followed by recommendations and
119 conclusions.
120

121 ## 2. Climate description

122 The thermal behavior of a building depends on external conditions such as the outdoor temperature,
123 outdoor humidity, and solar radiation with its environment. It depends heavily on meteorological and in
124 situ conditions. Study of the effect of sunspot on the cooling floor is proposed in this study for Oran and
125 Becher cities. The selection of cities is based on the specificity of the climate (solar deposit, temperature)
126 and the type of soil. Oran is a city in the northwest of Algeria. It enjoys a Mediterranean climate (temperate
127 climate) characterized by hot and dry summers and mild and humid winters. Bechar, it is an internal city
128 located in the North West Sahara with a dry climate. A large solar energy potential is available [28] where
129 approximately 2.5 MWh/m² of annual solar energy on the horizontal plane. It seems that the southern
130 regions have significant resources. Bechar with 2.1 MWh/m². year, can be considered as a potential
131 location for solar energy. Oran city receives solar energy of 1.8 MWh/m².year. Reader can refer to [28]
132 for further information about the location and climatic conditions of Oran and Bechar cities.
133 The minimum and maximum average temperatures and precipitation days of Oran and Bechar cities are
134 represented in figures 2-a and 2-b. The results show that the maximum outdoor temperature can go up to
135 42°C for Bechar city and 35°C for Oran city. Figures 2-c and 2-d shows the monthly number of sunny,
136 partly cloudy, overcast and precipitation days. Days with less than 20% cloud cover are considered as
137 sunny, with 20-80% cloud cover as partly cloudy and with more than 80% as overcast [29]. The results
138 indicate that the sky in July for Oran city is partly cloudy for 22 days. On the other hand, for Bechar city,
139 the sky is partly cloudy for only 5 days. For this purpose, we present in this study, the effect of cloud

quantity on the solar power received on the cooling floor, for the city of Oran. Details about sky state and average temperature are given in [29,30].

3. Methodology

Using a static coupling method between TRNSYS and FLUENT, the thermal behaviour of the sunspot and indoor air were accurately predicted. As shown in Figure 1, the methodology implemented in this paper followed a coupled approach involving CFD simulation and transient systems simulation program (TRNSYS).

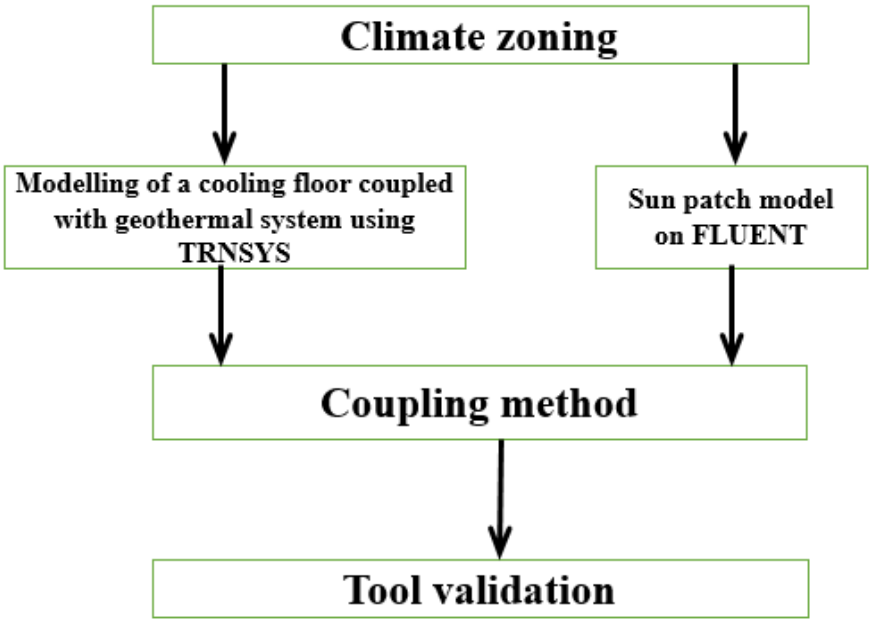

Figure 1: Conceptual framework for the study methodology

We first modelled the cooling floor coupled to the underground tank (UNT) using TRNSYS software. Secondly, we used the results obtained by TRNSYS tool, as inputs in FLUENT to predict the sunspot on cooling floor exchanging appropriate boundary conditions as shown on figure 2. The benefits provided by one tool are missing in the other tool, such that an 'optimum' model would be the complement of both tools, requiring a coupling strategy [31]. Indeed, FLUENT requires surface temperature and heat flux coefficients to describe the dynamic thermal behaviour of experimental cell, but these values are unknown

before realization. Moreover, we can get these parameters using TRNSYS which are more realistic and depend on the climatic conditions, the thermal properties of cell materials and the cooling source.

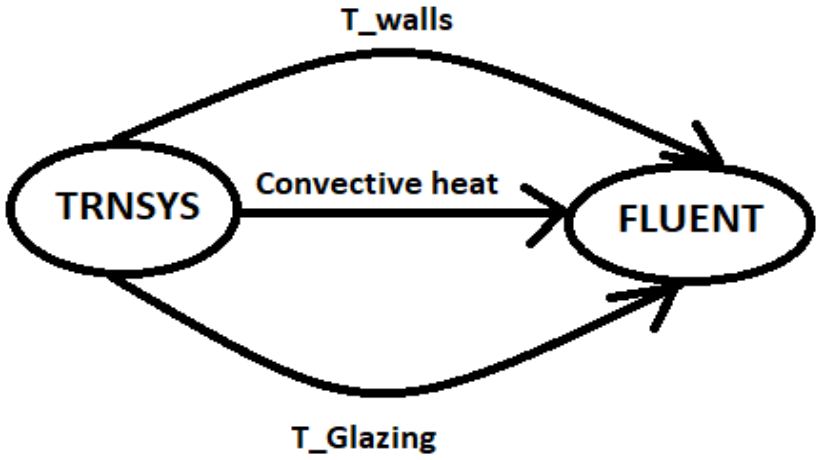

Figure 2: Co-simulation TRNSYS-FLUENT

Sunspot model developed in FLUENT allows to assess the sunspot localization, indoor air and floor temperatures and distribution of entering solar heat flux on the cooling floor for given period, orientation, geographic site and sunshine factor (figure 3). The solar ray tracing algorithm lets calculate the solar heat flux using a source term in the energy equation [32]. The solar load model's ray tracing algorithm can be used to predict the direct illumination energy source that results from incident solar radiation. It takes a beam that is modelled using the sun position vector [32].

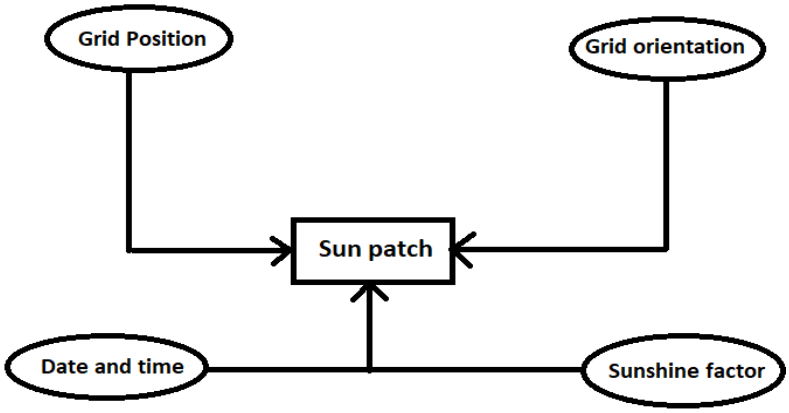

Figure 3: Flowchart for sunspot model identification

4. Experimental device

The system studied consists of an experimental cell equipped with a cooling floor coupled to an underground tank buried at a depth of 2 m with a total volume of 4 m^3, as shown figure 4-a. The experimental cell corresponds to two adjoining rooms (1 and 2) having the same geometric dimensions (Figure 4-b). The cell is located at the Institute of Civil and Mechanical Engineering of the University of Sciences and Technology of Oran, Algeria, where the coordinates are: 35.65° N, 0.62° W, with north-south orientation.

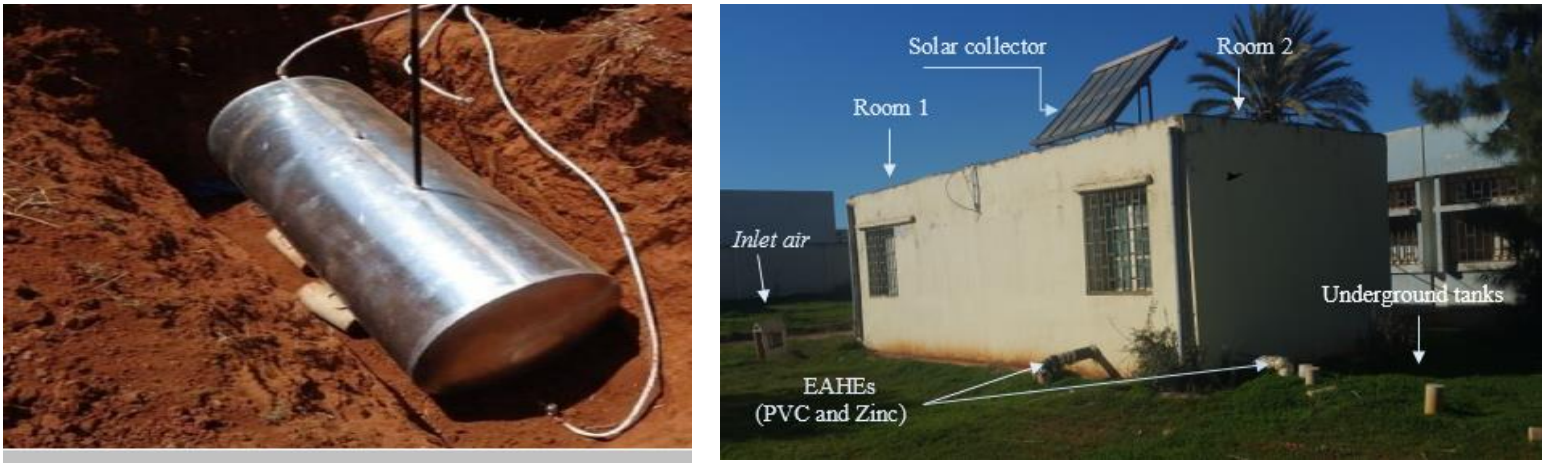

a- Underground tank **b- Experimental cell**

Figure 4: UNT under construction, installation and coupling with the experimental cell.

Several sensors were used (figure 5-a) to measure:

- The indoor air temperature for irradiated zone; position 1 (H=0.5 m) and position 2 (H= 1.4);
- The indoor air temperature for shaded zone position 3 (H=1.4m);
- The surface and inlet cooling floor temperatures (Positions 4 and 5);
- Outdoor temperature measured using a mini weather station (OREGON type).

184 Table 1 shows the characteristics of the measurement sensors used.

185 **Table 1** : Wireless sensor characteristics

Measured parameter	Measuring range **(Plage de mesure)**	Accuracy **(Précision)**	Type of sensor	Units
Temperature	- 40 °C < T°< 60 °C	± 1,5°C	Thermocouple	°C
Outdoor temperature	- 40 °C < T°< 60 °C	±1 °C	Weather station	°C

186

187 Temperature measurements were performed using K-type thermocouples. The experimental test is
188 equipped with a unit for displaying and recording measured data for a one-hour step. The collection and
189 storage of measured data is carried out through an acquisition chain (KEITHLEY 7700), which allows
190 the measurements taken at different points to be transmitted to a post-computer.
191 M. H. Benzaama et al., [11] studied the performance of seasonal storage without taking into account the
192 effect of overheating of the cooling floor. Temperature measurements were conducted only for the
193 occupied area (in the middle of the room). Temperature sensors have been placed to measure the
194 temperature of the illuminated zone as shown figure 5-b but they weren't exploited. These sensors make
195 it possible to compare between the thermal behavior of the umbrageous and illuminated zones.

196

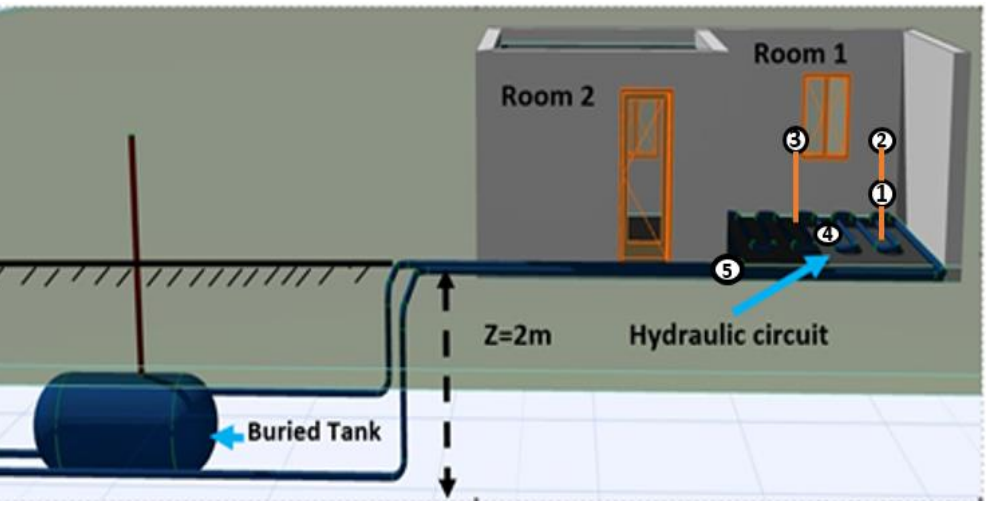

197 **a- Location of the thermocouples** **b- Sunspot location**

198 **Figure 5:** Experimental measures

199 The condition of the experimental cell construction is considered to be highly isolated and the thermal
200 properties of the exterior walls, partition, ceiling and floor are specified in Table 2.

201 **Table 2**: Thermal properties of cell materials.

Wall type and layer name (from inside to outside)	Thickness [m]	Conductivity [W/(m.K)]	Specific heat [kJ/(kg.K)]	Density [kg/m^3]
External and partition wall				
Cement-coating	0.01	1.15	1.0	1800
Brick	0.1	0.5	0.92	1100
Insulation	0.04	0.03	1.45	20
Brick	0.1	0.5	0.92	1100
Cement-coating	0.01	1.15	1.0	1800

Ceiling				
Cement-coating	0.01	1.15	1.0	1800
Ceiling block	0.16	1.14	0.65	1850
Concrete	0.04	1.75	0.92	2300
Insulation	0.02	0.03	1.45	20
Waterproofing coating	0.03	0.04	0.67	200
Floor				
Gerflex coating	0.003	0.31	1.046	1190
Concrete	0.1	1.75	0.92	2300
Insulation	0.04	0.03	1.45	20
Concrete	0.1	1.75	0.92	2300
Door				
lightwood	0.05	0.2	1600	600
Window				
Single glazed	0.004	1.2	830	2750

5. Numerical model

5.1 UNT coupled to cooling floor model

The UNT system is modelled by associating type 38 with type 711 (Figure 6). The association between these components allows modelling the thermal behavior of a water storage tank buried in the ground. The ground temperature for different burial depths of the tank is modelled using the Kusuda & Achenbach correlation. It is used to calculate temperature profiles in undisturbed soil at different depths. The model is based on the theory of thermal conduction applied to a semi-infinite homogeneous solid. The equation that provides soil temperatures at different depths is given as follows:

$$T(Z,t) = T_m - A_s\, exp\left(-Z\left(\frac{\pi}{365\,\alpha_{soil}}\right)^{1/2}\right)\mathrm{Cos}\left[\frac{2\pi}{365}\left((t-t_o)-\frac{Z}{2}\left(\frac{365}{\pi\,\alpha_{soil}}\right)^{1/2}\right)\right] \quad (1)$$

Where Z is the soil depth (m), t is the time (hour), t_0 is the time of year with minimum soil surface temperature (hour), T_m is the mean surface temperature (°C), A_s is the amplitude of soil surface temperature throughout the year (K), and α_{soil} is the soil thermal diffusivity (m^2/s).

The energy balance on a water node takes into account storage losses from the tank and conduction between segments, and this is written as follows:

$$\rho_w\, C_{p,w}\, V_i\, \frac{dT_i}{dt} = -(UA)_i(T_i - T_{env}) + (kA)_{i-1}\frac{(T_{i-1}-T_i)}{\Delta h_{i-1}} - (kA)_i\frac{(T_i-T_{i+1})}{\Delta h_{i+1}} \quad (2)$$

where ρ_w is the water density (kg/m^3), $C_{p,w}$ is the heat capacity of water (J/kg K), UA is the overall loss coefficient (W/k), T_{env} is the environmental temperature and Δh is the separation between centers of segments.

The total loss from the tank is written as follows:

$$\dot{Q}_{env} = \sum_{i=1}^{N}(UA)_i\,(T_i - T_{env}) \quad (3)$$

The energy input to the tank due to the cold inlet flow is given as follow:

$$\dot{Q}_{in} = \dot{m}\;\; C_{p,w}\,(T_{inl} - T_{outl}) \quad (4)$$

For cooling floor surfaces, the convective heat transfer coefficient is calculated using Type 80 by this Eq.5:

$$\alpha_{conv} = 2.11\left(T_{surf} - T_{air}\right)^{0.31} \quad (5)$$

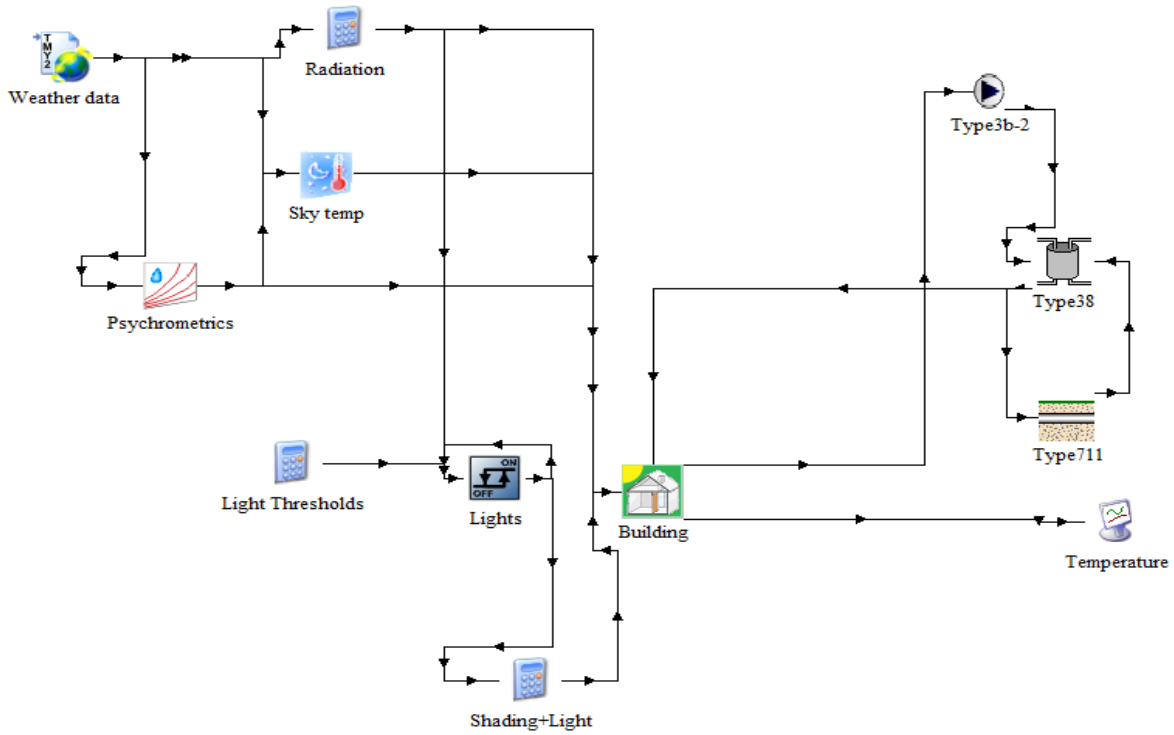

Figure 6: Simulation flow chart in TRNSYS space.

5.2 Sunspot model:

Where surfaces exposed to the sun, solar radiation heat transfer is considered. For solar radiation, FLUENT software provides solar radiation calculation model using the Solar-Ray Tracing method. The resulting heat flux that is computed by the solar ray tracing algorithm is coupled to the FLUENT calculation via a source term in the energy equation [32]. The solar load model's ray tracing algorithm can be used to predict the direct illumination energy source that results from incident solar radiation. It takes a beam that is modelled using the sun position vector [32]. This model can be used to visualize the dynamic thermal behaviour of indoor air and surface cooling floor relative to the sunspot shifting for a given time and location. The model of turbulence used in this study is K-ε Standard for steady-state and Boussinesq approximation has been used in this case.

The two illumination parameters used to describe the intensity of the solar load consist of two irradiation terms, direct solar irradiation and diffuse solar irradiation. The direct solar irradiation uses a two-band spectral model and accounts for material properties in IR- and visible bands. The diffuse solar irradiation uses a single-band hemispherical averaged spectral model only present in actual sun light [33].

The inputs for the Solar Calculator are given below:

Global position (latitude, longitude, and time zone), starting date and time, orientation of the building, solar irradiation method and Sunshine factor.

The sunshine factor accounts for the cloud covering the sky at a given time and location under study. so it is basically percentage of cloud cover which range from 0 to 1 where 0 means completely covered with cloud and 1 means no cloud. The cloud cover basically reduces the sunlight from sun. The sunshine factor is simply a linear multiplier that allows the incident load to be reduced in order to account for cloud cover. Once the irradiation and solar beam direction are known, they are applied as inputs to the solar ray tracing algorithm or the discrete ordinates method [34, 35].

The direct normal irradiation that is calculated using NREL's Solar Position and Intensity Code (Solpos) given in [32]:

$$E_{dn} = S_{entrn} \cdot S_{unprime} \tag{7}$$

Where S_{etrn} is the direct normal of the solar irradiance.

$S_{unprime}$: the correction factor used to reduce the solar load through the atmosphere.

The equation of diffuse solar irradiation for surfaces other than vertical surfaces is given by [32]:

$$E_d = C.E_{dn}.\frac{(1+\cos \varepsilon)}{2} \tag{8}$$

Where ε : tilt angle of the surface (in degrees) from the horizontal plane.

Both absorptivity and transmissivity are defined for normal incident angle to the surfaces but are recomputed in FLUENT to represent the correct angle. Glazing of materials can also be included when using solar ray tracing [33]. For this to work the transmissivity and reflectivity has to be specified in the wall boundary conditions. Table 3 and 4 represent the composition of window and the surface radiation properties of glass.

Table 3: Composition of window.

Material	Conductivity, λ (W/m.K) (at 20 °C)	Heat capacity, c_p (J/Kg.K)	Density, ρ (Kg/m^3)
Single glazed window	1,2	830	2750

Table 4: The surface radiation properties [36]

Emissivity		0.90
Absorptivity	Visible (αV)	0.49
	IR (αIR)	0.49
	Diffuse(αD	0.49
Transmissivity	Visible (vV)	0.30
	IR (vIR)	0.30
	Diffuse (vD)	0.32

Solar ray tracing can be combined with one of the available radiation models called Surface-to-Surface when the effect of surface emissions is important. The solar ray tracing algorithm functions as the source of solar heat and the S2S radiation model takes into account the energy diffused indoors [33]. The S2S radiation model is based on a calculation that takes into consideration the characteristics of the included irradiating surfaces in relation to each other [33]. The combination of these models give a realistic thermal behavior of building.

The energy equation used in the S2S model is composed of directly emitted and reflected energy. The energy reflected from a surface is dependent on the energy incident on the surface and can thus be expressed as a function of the energy flux leaving all radiating surfaces [33] as shown figure 7. The energy flux from surface k is described as:

$$q_{out,k} = \varepsilon_k + \sigma T_k^4 + \rho_k q_{in,k} \quad (9)$$

where $q_{out,k}$ represents the energy flux leaving the surface, $q_{in,k}$the energy flux incident on the surface, ρ_k the reflected energy, ε_k the emissivity, σ is the Boltzmann's constant and T is the temperature.

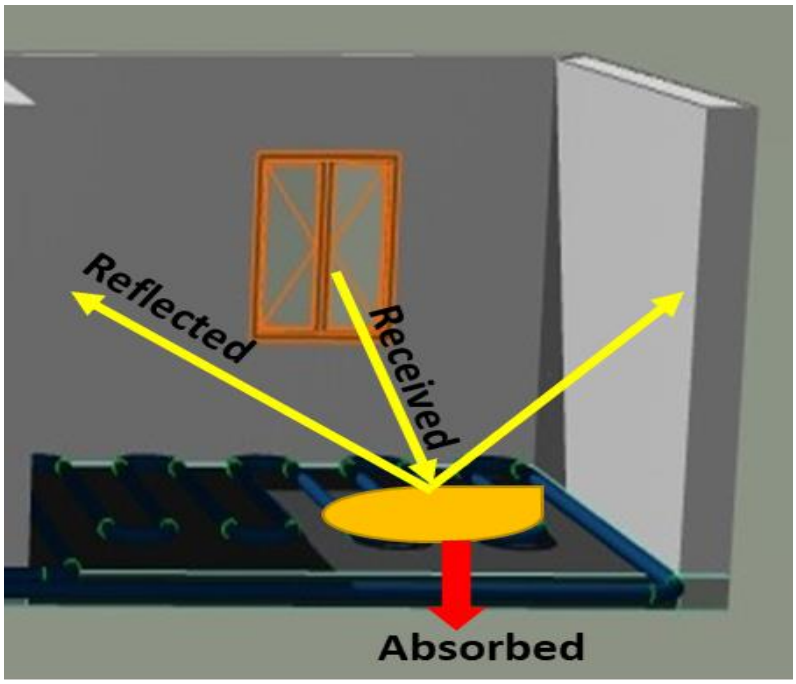

Figure 7: Solar radiation distributions

Since then, all boundary conditions were determined and the main of them are shown in Table 4. The thermal characteristics of the wall surface are very important parameters for the calculation of the radiant heat transfer of the indoor walls, as shown in Table 5.

300 **Table 5**: Boundary conditions.

	At 12 pm		At 3 pm	
Wall	Temperature °C	Heat convection coefficient ($W/m^2.K$)	Temperature °C	Heat convection coefficient ($W/m^2.K$)
North Wall	23.41	/	24.01	/
South Wall	23.39	/	24.02	/
Est Wall	23.49	/	23.98	/
West Wall	23.39	/	24.01	/
Floor	23.16	0.2	23.45	0.2
Ceiling	23.49	/	24.01	/

301

6. Results and discussion

6.1 Experimental results

We present in this section the experimental data for the period of July 2014. We follow for 10 days, the inlet temperature, cooling surface temperature and outdoor air temperature as shown in figure 8. The results show that the temperature difference beteween the inlet temperature and outdoor temperature is around 12 °C. This difference in temperature can supply the heat energy required to ensure a best thermal comfort. The cooling floor surface temperature does not exceed 25 °C which corresponds to the criteria of thermal comfort [37].

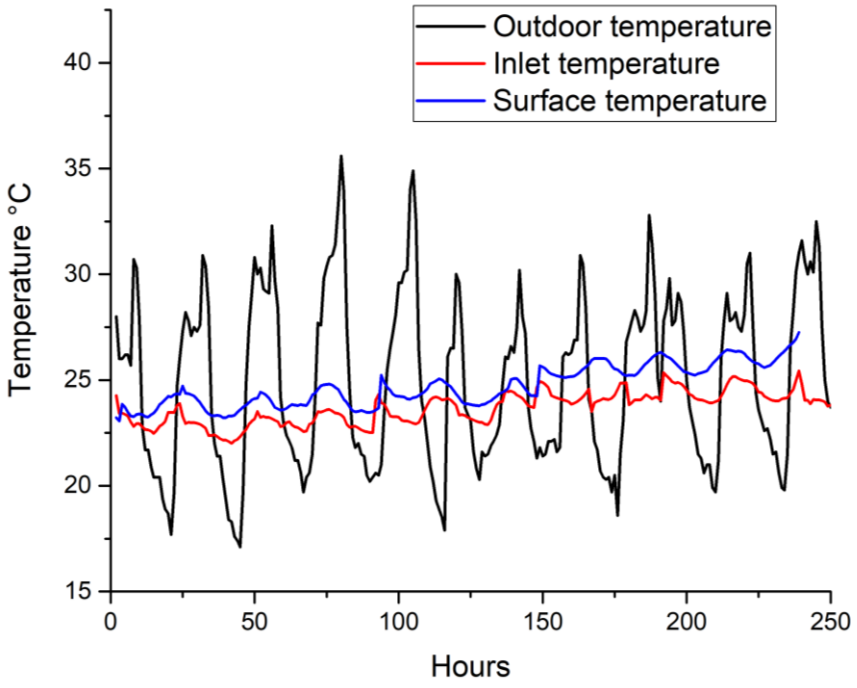

Figure 8: Experimental measurements of the surface temperature and inlet temperature of the cooling floor

Figure 9 shows the indoor air temperature evolution at two different zones. In the study of M. H. Benzaama et al., [11] the authors presented only the temperature of the shaded zone (Position 3). The area near the window which is influenced by solar radiation is neglected. The results of figure 9 show that thermal behaviour of positions 1, 2 and 3 is different. Sensors 1 and 2 are

influenced by the presence of sunspot. The irradiated surface emits a heat flow that causes overheating of the air zone where sensors 1 and 2 are placed. Figure 11 shows a temperature heterogeneity between positions 1, 2 and position 3. The temperature of the indoor air is not homogeneous in the room. The indoor air temperature in the irradiated zone (Positions 1 and 2) reaches a maximum value of 28 °C. On the other hand, the indoor air temperature in the occupied zone (Position 3) takes an average of 24 °C which corresponds to the criteria of thermal comfort (Upper limit for the operative temperature in summer is 26°C [32]). A temperature difference of 4 °C between the two zones can cause a temperature heterogeneity in the room (Discomfort).

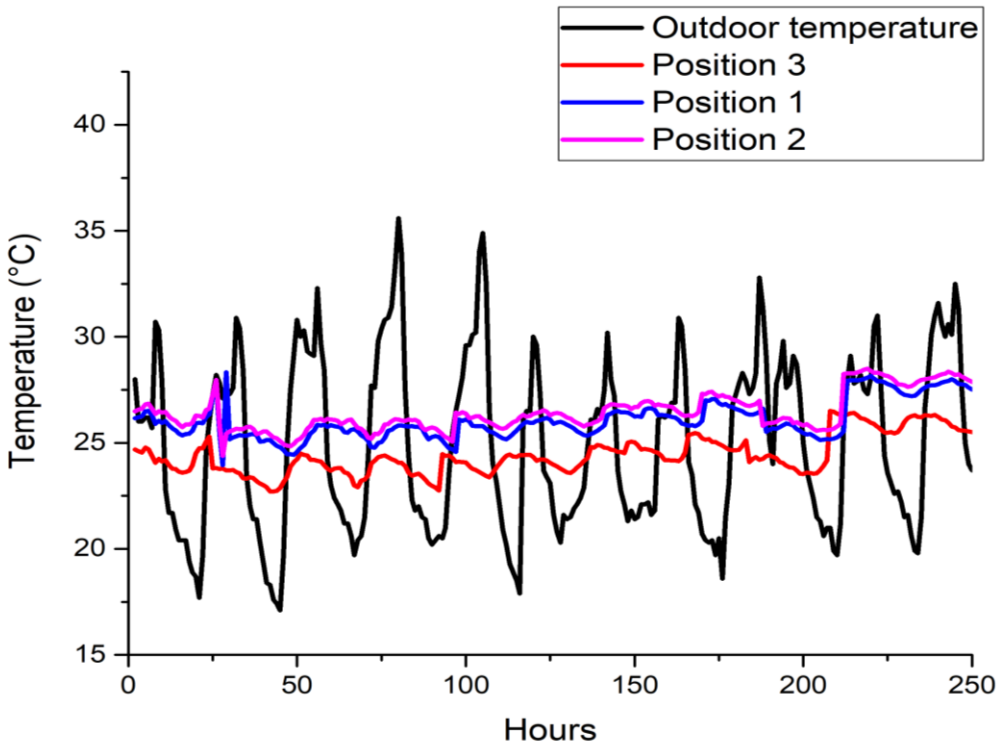

Figure 9: Experimental measurements of indoor air temperature for the umbrageous and illuminated zones.

6.2 Model validation

Firstly, we present in figure 10, the cooling needs of the experimental cell estimated by numerical simulation using TRNSYS tools for a period from May to September. It can be seen that the need is high during the summer season and especially during the month of July with a value of 379.6 kWh. For this purpose, the choice of the period of the measuring campaign corresponds to the period in which the cooling needs are important.

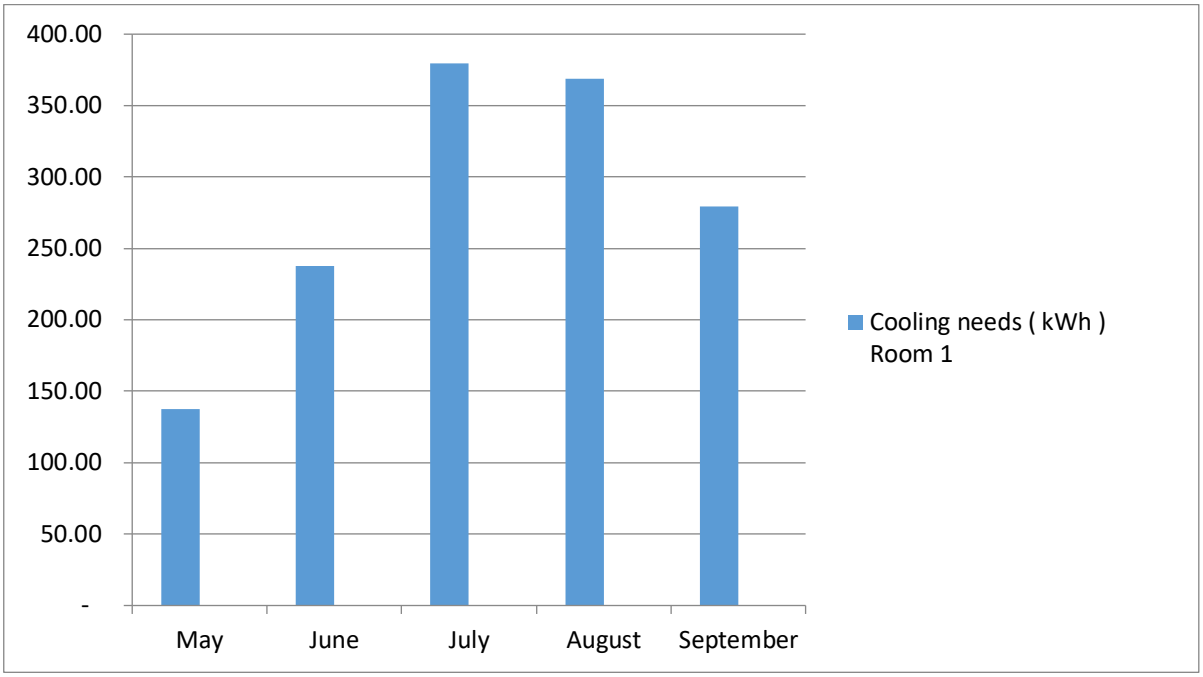

Figure 10: Cooling needs

We present in this section the validation of the two models TRNSYS and FLUENT. As presented in the methodology, the geothermal system and the experimental cell are modelled on TRNSYS. TRNSYS model was validated using an experimental data. Figure 11 show that the simulation results in good agreement with the experimental data, wherein the deviation between them falls within 0.5 °C. The indoor air temperature obtained by TRNSYS is compared with the temperature of the umbrageous zone. This temperature is considered uniform throughout the room, but that does not reflect reality. The models existing in the literature such as TRNSYS validates only the temperature of the occupied area (Position 3).

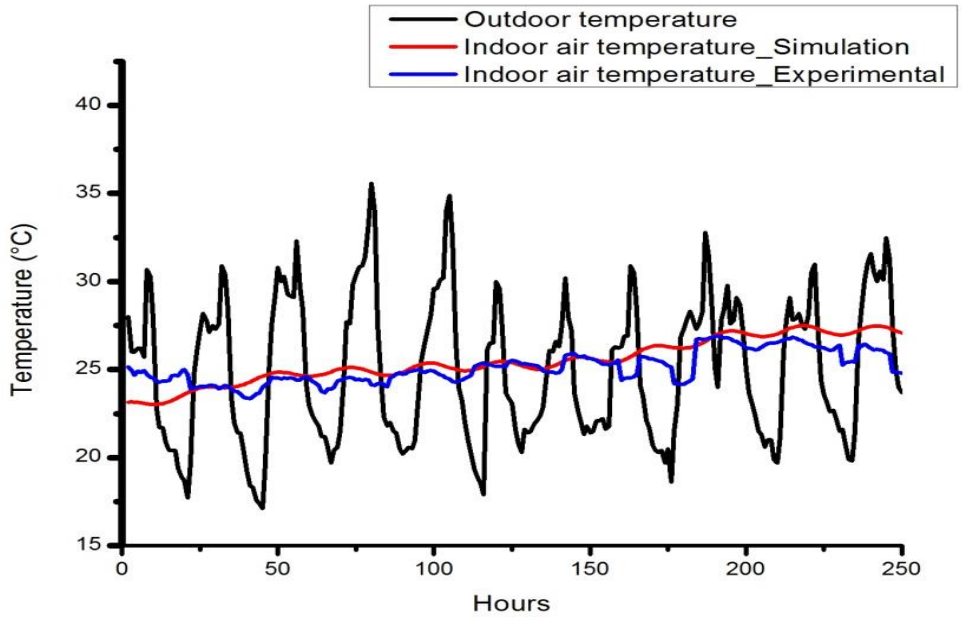

Figure 11: Experimental indoor air temperature and simulation

The validation of the illuminated zones was focused on the comparison of vertical air temperature distribution (figure 12-a). The simulated results were compared with the measured data (positions 1 and 2) towards the vertical direction as shown figure 12-b. The results show comparisons of the temperature difference between experiments and simulations from cooling floor surface to 1.4 m high. The boundary conditions of validations of model were measured at 12 am on July 07. From these results, it can be noted that the two temperature profiles have an almost similar trend, which confirms a good agreement between the simulated data and the collected data.

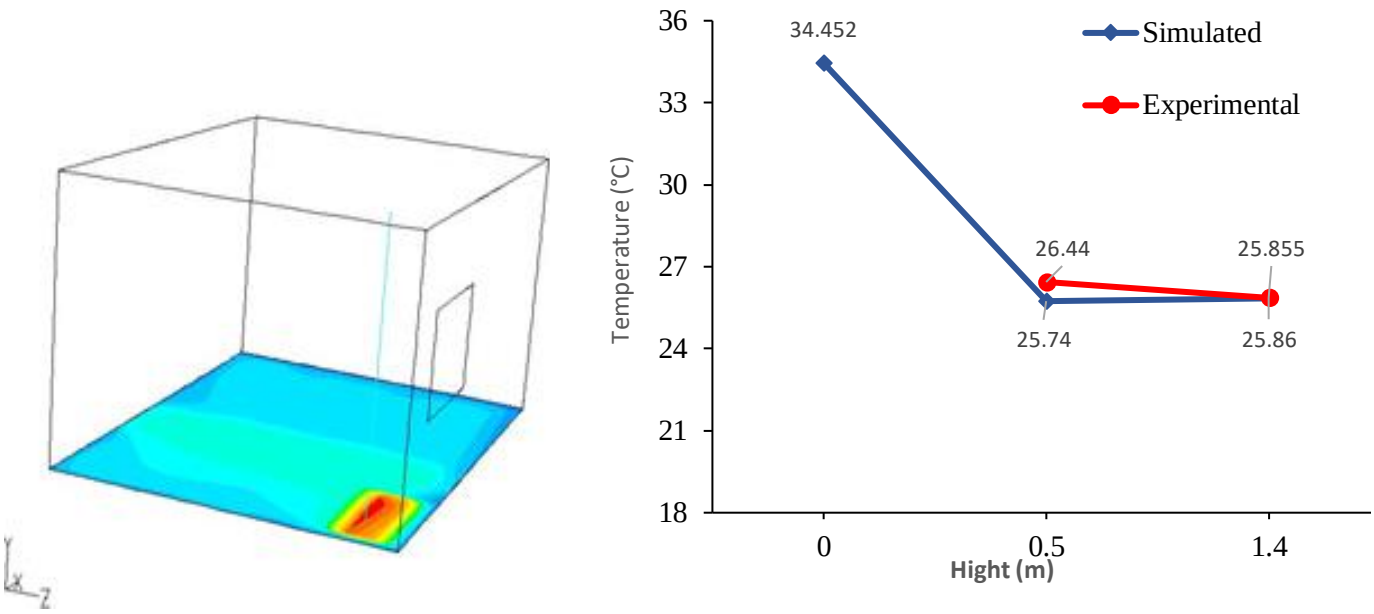

a- Sunspot location **b- Model validation**

Figure 12: Comparisons between experimental and simulated air along the Y-axis at 12 am on July 07

Experimental studies usually involve unpredictable and uncertain factors that occur due to instrumental, calibration, and human measurement errors. These uncertainties may be calculated using statistical analysis through recognized formulae. For this, the error analysis of the thermal model performance of the experimental cell was calculated by comparing its results with the experimental data. In this study, the Normalized Mean Bias Error (NMBE) and the Coefficient of Variation of the Root Mean Square Error (CV(RMSE)) were calculated. They are defined as follows:

$$\mathrm{NMBE} = \frac{1}{\bar{m}} \frac{\sum_{i=1}^{n}(m_i - s_i)}{n-P} \; X \; 100(\%) \qquad (10)$$

$$\mathrm{CV(RMSE)} = \frac{1}{\bar{m}} \sqrt{\frac{\sum_{i=1}^{n}(m_i - s_i)^2}{n-P}} \; 100\ (\%) \qquad (11)$$

Where $\bar{m}$ giving the global difference between the real values and the predicted ones, p is the number of adjustable model parameters, which, for calibration purposes, is suggested to be zero,

n the number of measured data points, m_i is the measured variables, and s_i is the simulated variables. The (CV(RMSE) and NMBE of indoor air temperature reported in Table 6. The results obtained, corresponds to the criteria of ASHRAE Guideline 14.

Table 6: Performance of the model.

Data Type	Index	ASHRAE Guideline 14 [38,39]	Present study
Calibration criteria			
Hourly criteria %	NMBE	$\pm$ 10%	-2.55%
	CV (RMSE)	$\pm$ 30%	3.8%

Figure 13 illustrates the impact of thermocouple uncertainty on the indoor air temperature, using error bars. Error bars are graphical representations of the variability of data and used on graphs to indicate the error or uncertainty in a reported measurement. They give a general idea of how precise a measurement is, or conversely, how far from the reported value the true (error free) value might be. Error bars often represent one standard deviation of uncertainty, one standard error, or a particular confidence interval [40]. A range of uncertainty has been defined according to the accuracy of the temperature sensors (± 1.5°C) as shown in figure 15. The results show the error range of the experiment (measured indoor temperature ± 1.5°C) and the simulated temperature. In general, the simulated indoor air temperature fluctuates within the uncertainty range except between 176h - 197h (figure 13). In this period, we notice a disturbance in the measurement of indoor and outdoor temperatures. Temperature peaks and drops are observed which are probably due to the acquisition chain.

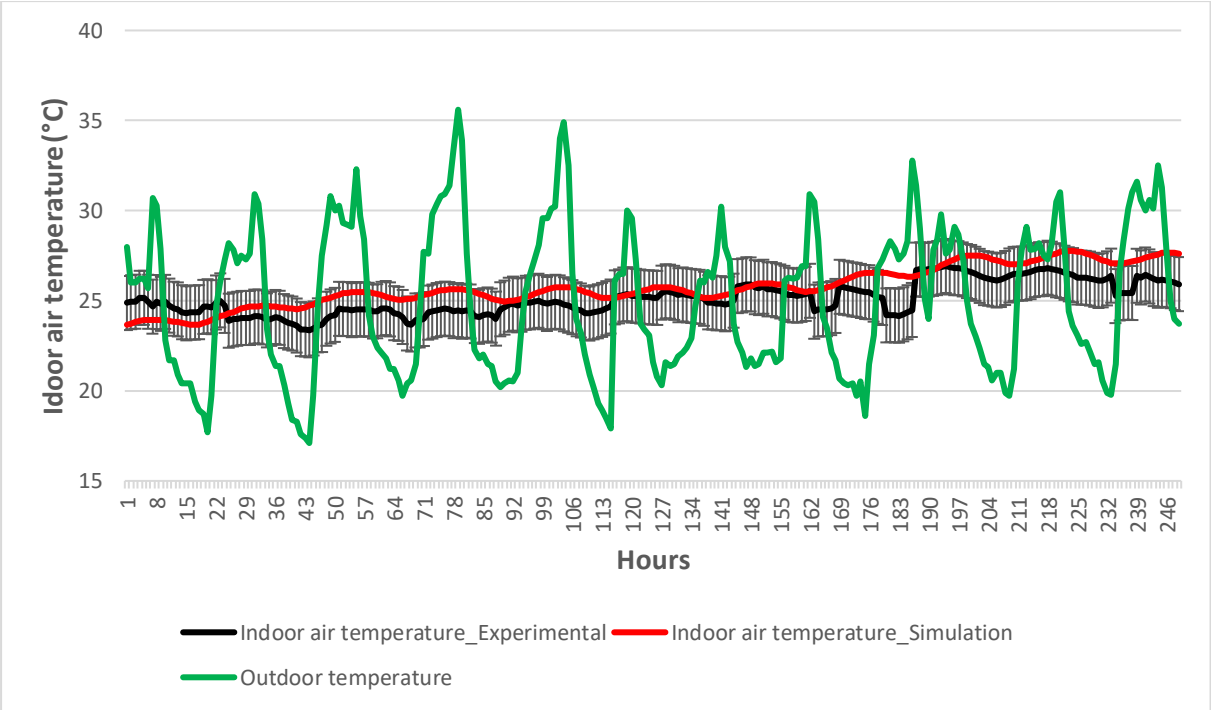

Figure 13: Error bars analysis

The total uncertainties of the indoor air were therefore mainly determined by the uncertainty of the input parameters. Supposing that each single input parameter is independently of other inputs, the uncertainty can be estimated from CV(RMSE) and NMBE. Table 7 illustrates the effect of the uncertainties of some parameters on the uncertainties of indoor air temperature. These were found using TRNSYS simulations. The uncertainties arose due to deviations of the model geometry or due to uncertainties in the calculation heat transfer. It can be noticed that results are very sensitive to wall insulation thickness. An increase of 5% of wall insulation thickness reduces the NMBE to -0.82% and the CVRMSE to 2.51%.

Table 7: Sensitivity of indoor air temperature to changes of important input parameters

Input parameter	Change of input parameter (%)	NMBE (%)	CVRMSE (%)
Slab concrete	+ 5	-2.36	3.57
Slab concrete	- 5	-2.48	3.95
Wall insulation	+ 5	-0.82	2.51
Wall insulation	- 5	-5.24	6.9
Infiltration	+ 5	-2.66	3.84
Infiltration	- 5	-2.43	3.73
Roof insulation	+ 5	-2.53	3.77
Roof insulation	- 5	-2.56	3.79

6.3 Coupling TRNSYS-FLUENT

6.3.1 Sunspot on cooling floor

The models presented in the literature cannot be generalized for all case studies since the distribution of entering solar heat flux on the cooling floor is imposed. We show in Figure 14 the sunspot position at 12 am and 13 p.m on July 07 for Oran city conditions (Mediterranean climate). Distribution of entering solar heat flux on cooling floor is around 120 W/m^2 and 110 W/m^2 at 12 a.m and 3 p.m respectively as shown in figure 14-a, c. We observe that sunspot moves from plane X = 1 at 12 a.m. to plane X = 2 at 3 p.m. causing superheating as shown figure 14-b, d.

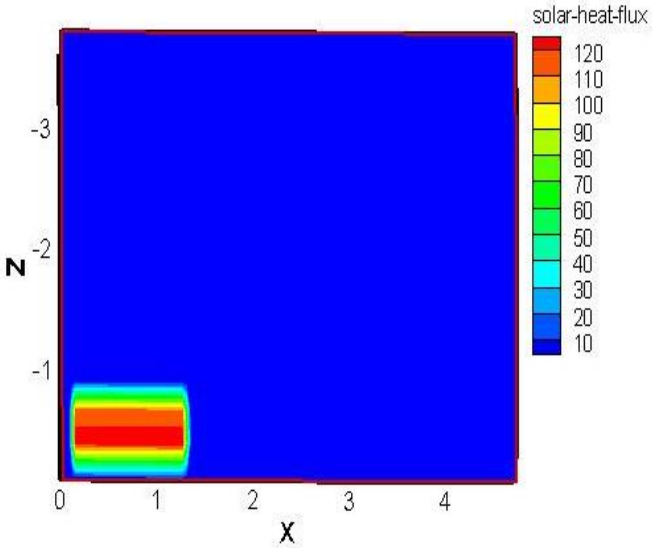

a- Solar heat flux

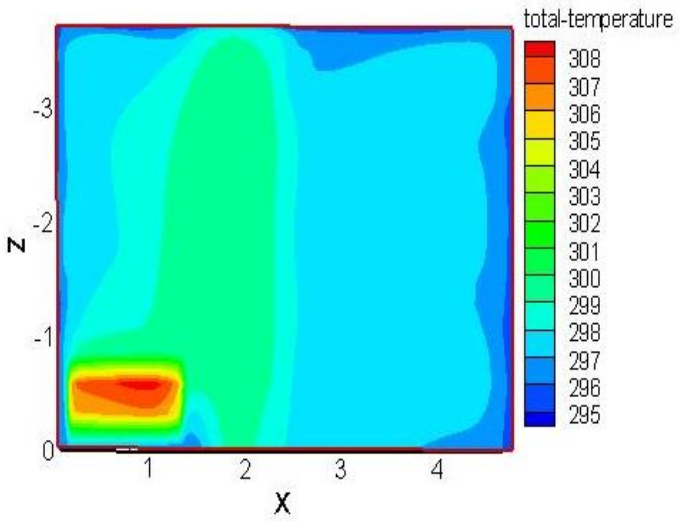

b- Surface temperature

At 12 a.m.

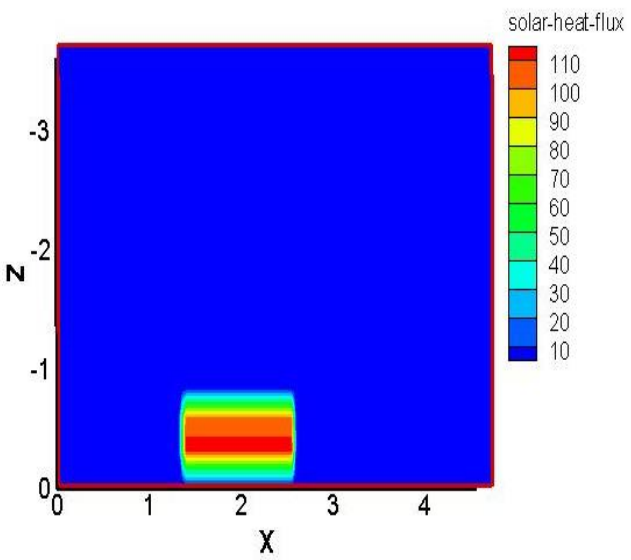

c- Solar heat flux

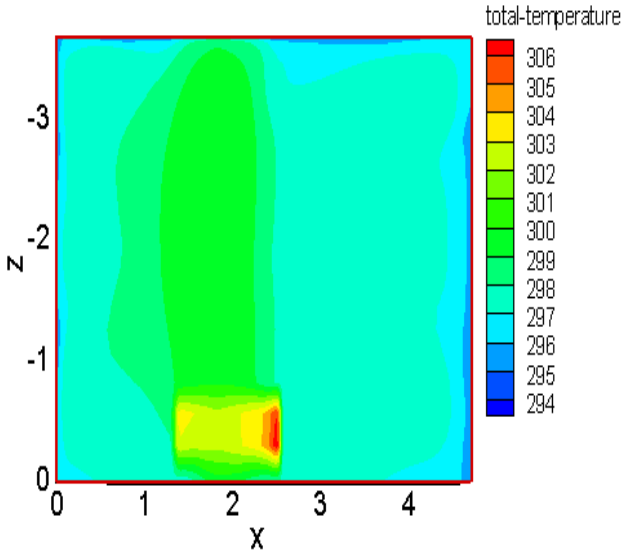

d- Surface temperature

At 3 p.m.

Figure 14: Solar heat flux (W/m^2) and surface temperature (K) of cooling floor

The developed model allows to plot the surface temperature and solar heat flux distribution along a line (We take Z = -0.5 along the X axis) as shown figure 15. For 120 W/m^2 of solar heat flux received on cooling floor, the effect of the sunspot shifting on the experimental cell are more remarkable for the surface temperature variation. During this period, some pics were observed. A superheating of 35°C at 12 a.m. and 33°C at 3 p.m was observed, which gives a wide temperature range of 13°C and 11°C in comparison with the umbrageous area respectively. Sunspot shifting from 12 p.m. to 3 p.m is done for a small distance, that has an effect on floor thermal inertia which causes superheating for a long period.

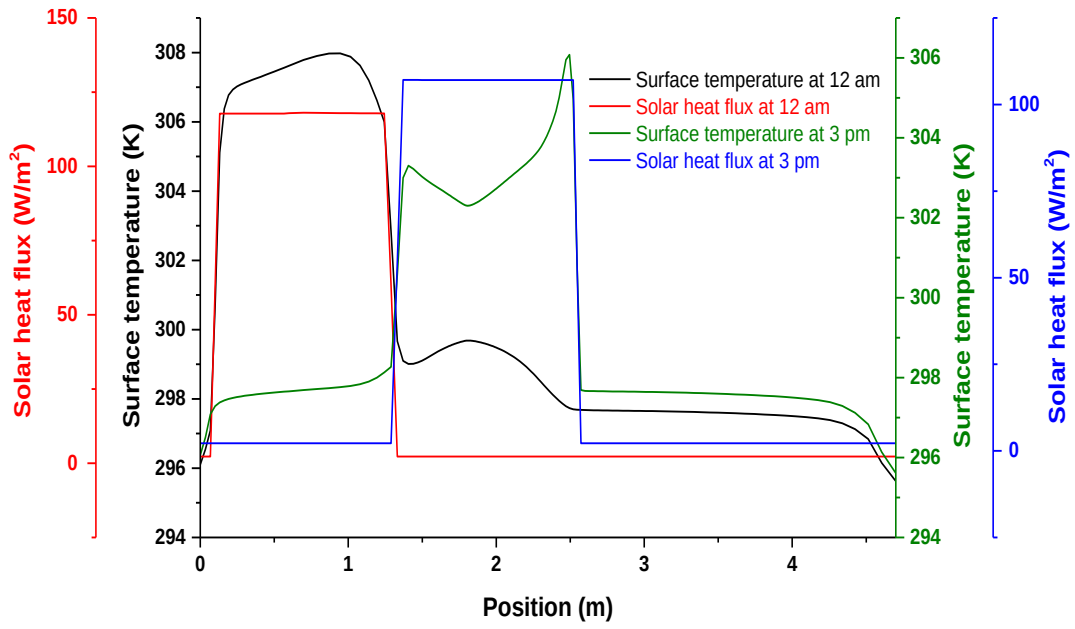

Figure 15: Surface temperature and solar heat flux on cooling floor at different time.

The incident solar radiation received on the cooling floor is redistribute due to absorption / emissivity of internal surfaces. For this purpose, we present in Figure 16 the reflected IR radiation compared to the solar radiation received on the cooling floor. For the metrological conditions of Oran and at 12 am, the reflected IR radiation is of the order of 15 W/m^2 which

gives 105 W/m^2 of absorbed solar radiation. An important value that could influence the indoor air temperature for a long period of time.

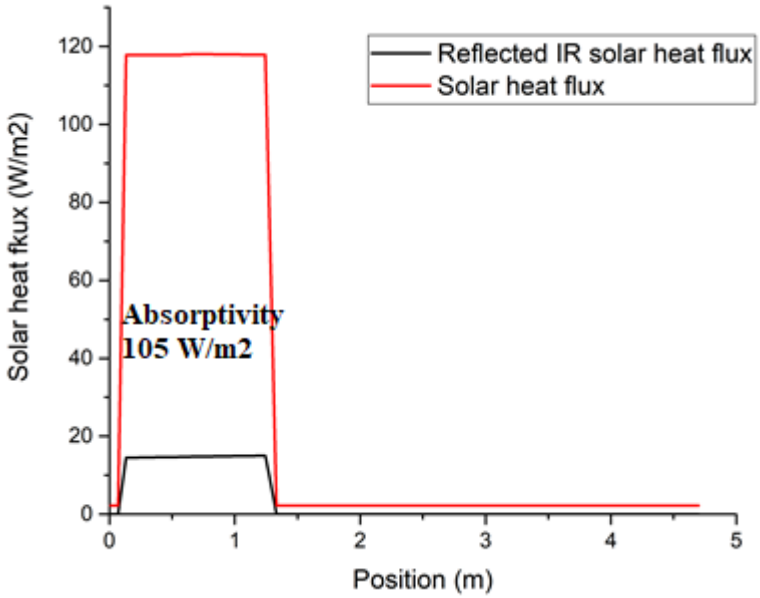

Figure 16: received and reflected solar radiation

Due to high-intensity solar radiation absorbed and reflected, the dynamic thermal behaviour of indoor air temperature in the irradiated zone could be much higher than that in shaded zone. This results allow to evaluate the solar power that influences the cooling capacity and the dynamic thermal behaviour of the indoor air. In this purpose, we present in the next section, the influence of reflected radiation of sunspot on the dynamic thermal behaviour of indoor air.

6. 3.2 Dynamic thermal behavior of indoor air

Figure 17 shows the indoor air temperature distribution in three different planes in July 07. At 12 a.m., heat transfer is observed from the sunspot to the cold surface of the cooling floor (Figure 17-a). The influenced area at 12 a.m. is larger than that at 3 p.m. Consequently, the influenced air volume at this plane ($0 < X < 2$) at 12 a.m. is greater than that at 3 p.m (Figure 17-b). The indoor air temperature in this plane is around 28°C. The thermal behavior at the second and third plan is identical at 12 a.m. and 3 p.m. The indoor air temperature in the

occupied area (X = 3) is around 26 °C and that of the umbrageous area (X = 4) is around 24°C. The temperature range can go up 4 °C which confirms the experimental results.

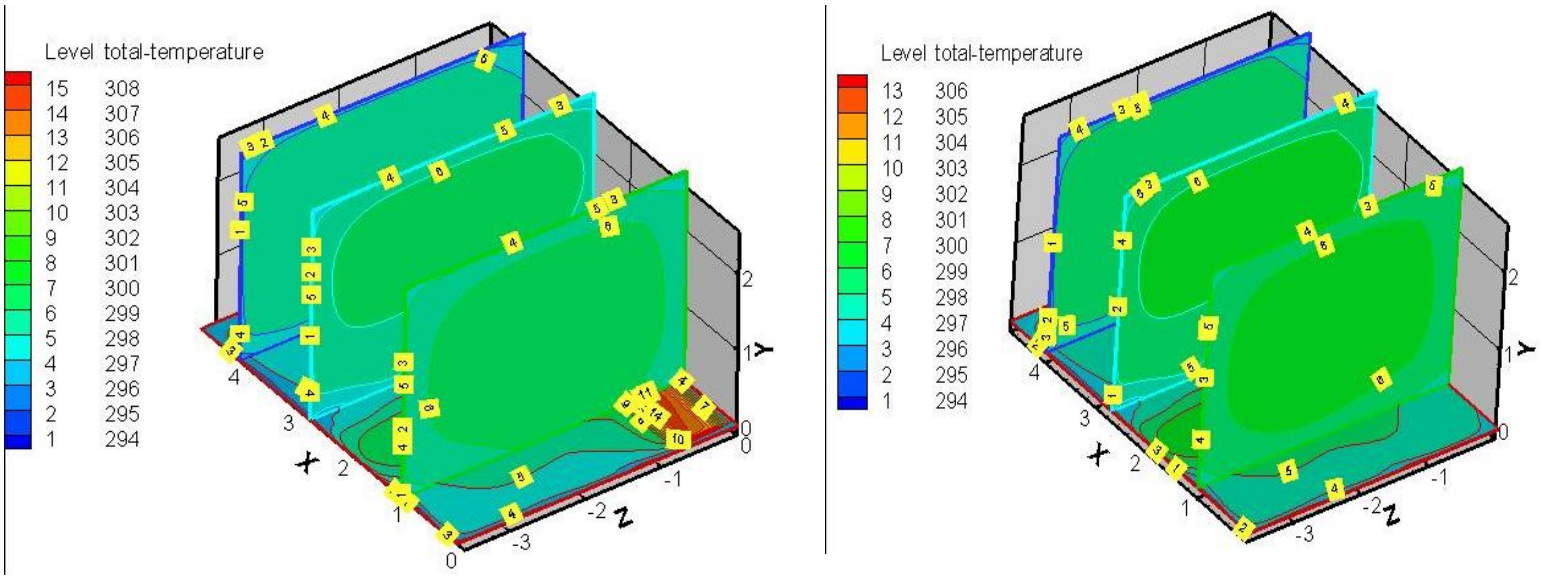

a- At 12 a.m. **b- At 3 p.m.**

Figure 17: Thermal behavior of indoor air with existence of sunspot at different planes (K)

Figure 18 shows that the plane 0 < X < 2 is influenced by the sunspot passage from 12 a.m. (Figure 18-a) to 3 p.m (Figure 18-b). At this level, the dynamic behavior is not the same between 12 a.m. and 3 p.m. The air velocity varies between 0.06 and 0.1 m/s. On the other hand, the dynamic behavior at the second and third plan is almost the same at 12 a.m. and 3 p.m. The air velocity in the occupied area (X = 3) is around 0.1 m/s, and that of the umbrageous area (X = 4) is around 0.06 m/s.

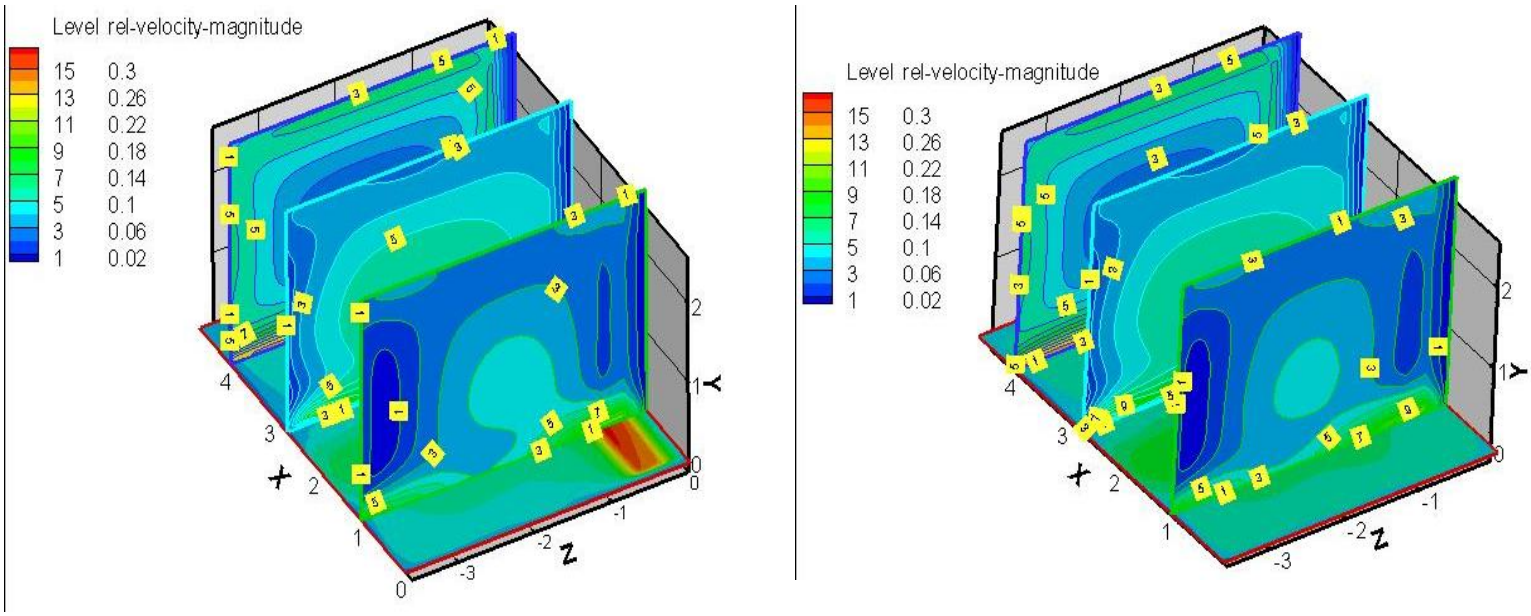

a- At 12 a.m. **b- At 3 p.m.**

Figure 18: Dynamic behavior of indoor air with existence of sunspot at different planes (m/s)

6.3.3 Effect of clouds on sunspot

Controlling solar energy therefore requires knowing the correct position of the sun (height and azimuth) as well as the intensity of radiation at any given moment, which depends on the clouds quantity. In this section, we present the effect of the clouds quantity on the sunspot (sunshine factor). The focus is on the solar heat flux received on the cooling floor and its effect on the thermal behaviour of the cooling floor and indoor air. Three case studies are presented: Case 1 with 0% cloud, case 2 with 50% of cloud, and case 3 with 80% of cloud as shown figure 19.

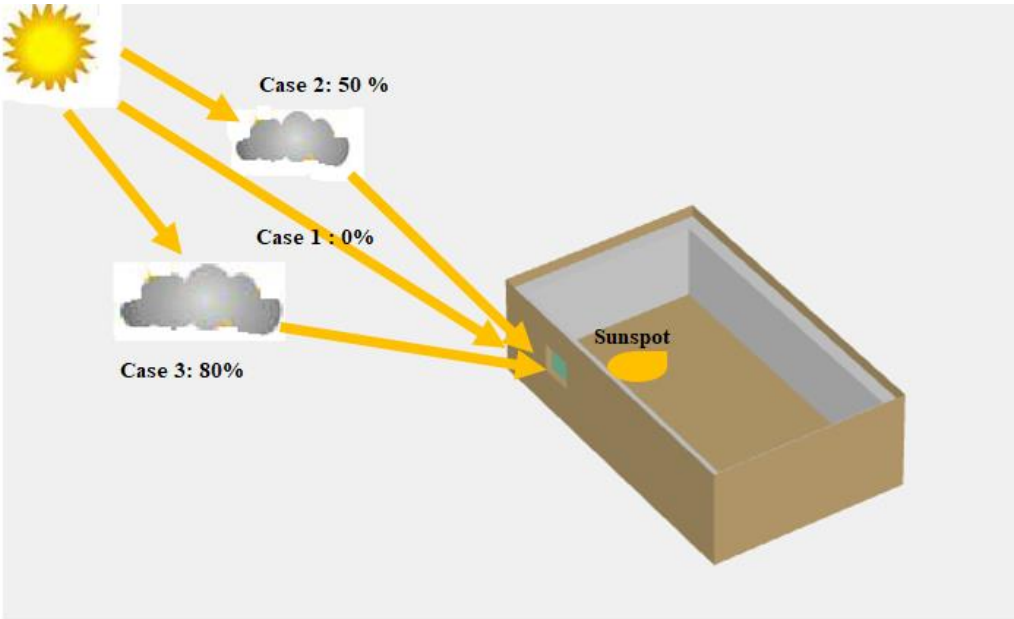

Figure 19: Illustration of the three case studies

Figure 20 shows the solar heat flux received on the cooling floor for the three case studies. The interest of this section is to show that the model not only allows to evaluate the solar heat flux received on the cooling floor in relation to the climatic conditions, but also in relation to the sky state (cloudy or clear sky). The results show that the solar heat flux received on the cooling floor for a cloudy sky (50% and 80% clouds) is in the order of 75 W/m^2 and 32 W/m^2 respectively. A difference of 88 W/m^2 between a clear sky (120 W/m^2) and an 80% cloudy sky.

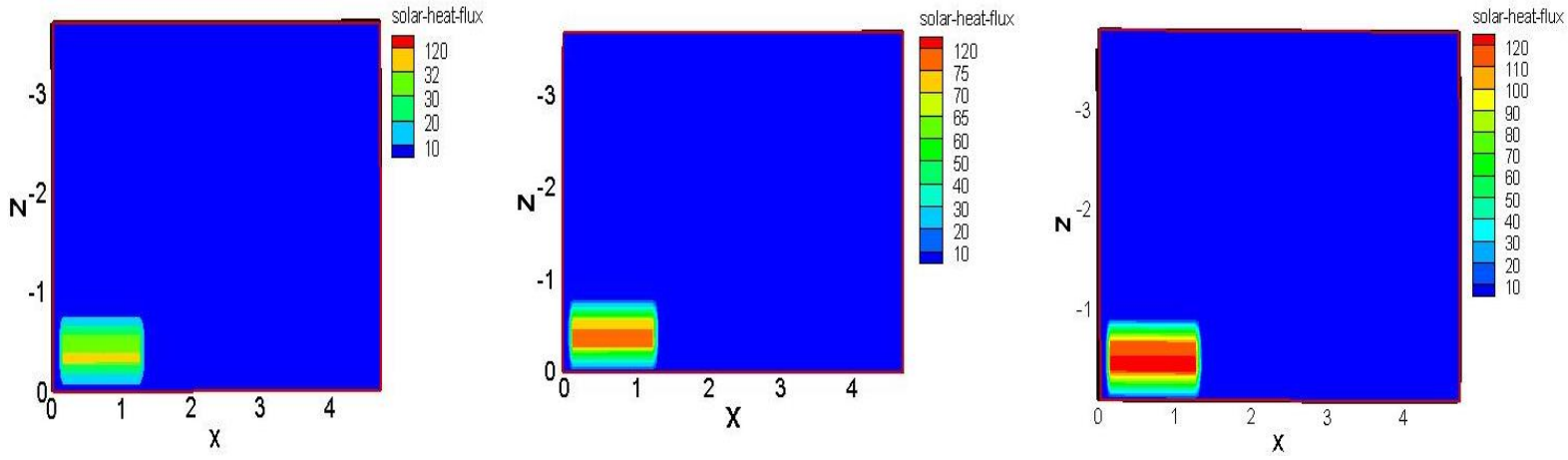

Case 3 : 80% clouds **Case 2 : 50% clouds** **Case 1 : 0% clouds**

Figure 20: Solar heat flux (W/m^2) received on the cooling floor

The solar heat flux received on the cooling floor for the three case studies causes a different thermal behaviour of cooling floor. The sunshine factor is an important parameter that is neglected in the numerical sunspot models mentioned above. This factor allows to predict the exact power received and transmitted to the indoor air, which allows to quantify precisely the overheating due to the sunspot. Figure 21 shows that for the same day of July 7th at noon and for the climatic conditions of Oran, the overheating of the cooling floor due to the presence of the sunspot is different. For cloudy sky (50% and 80%) the overheating is of the order of 31 °C and 27 °C respectively. On the other hand, the surface temperature of the cooling floor for a clear day is of the order of 35 °C. A temperature difference of 8 °C between a clear sky and a cloudy sky.

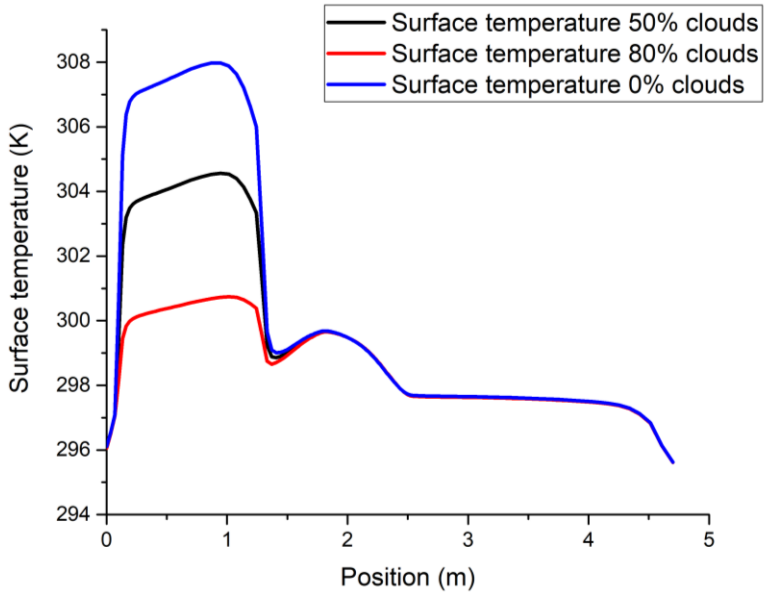

Figure 21: Surface temperature of the cooling floor for a cloudy and clear sky (Z= -0.5 along the X axis)

Therefore, part of the solar heat flux is reflected, disturbing the thermal behaviour of the indoor air. The results of figure 22 show that for a cloudy sky of 50% and 80% clouds, the reflected IR solar radiation is of the order of 9 and 4 W/m^2 respectively. A difference of 11 W/m^2 between a clear sky and cloudy sky.

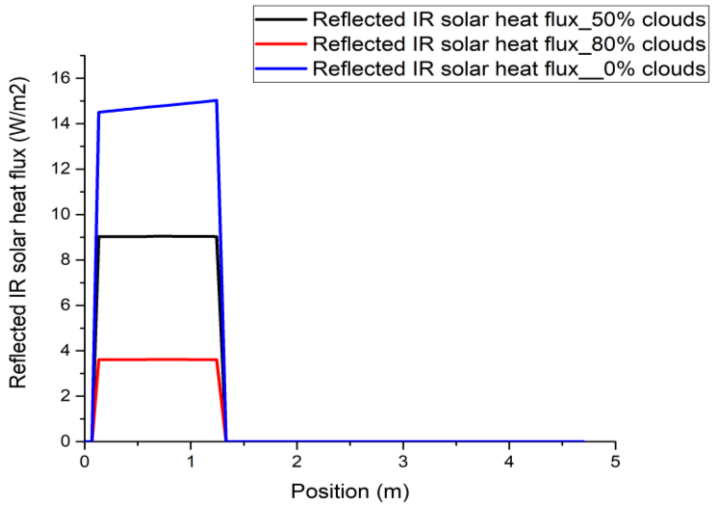

Figure 22: Reflected IR solar radiation for a cloudy and clear sky (Z= -0.5 along the X axis)

The temperature of the air around the irradiated area has a great effect on the thermal sensation of the human body. Figure 23 shows the cooling floor temperature, and the indoor air temperature around the irradiated area for the three cases. From figure 23, it is obvious that the surface temperature of the cooling floor in case 1 is more important than cases 2 and 3. This is due to the high solar heat flux received in the first case (See figure 20) compared to the other cases. A very high heat concentration on the cooling floor in the first case is observed compared to the cases 2 and 3. Therefore, this irradiated surface in case 1 radiates more heat (reflected IR solar radiation) to the indoor air, as shown in the figure 24. The reflected IR solar radiation, one of the most important factors that affect the air around the irradiated surface. Figure 23 shows that the thermal behaviour of the indoor air in the irradiated zone is not the same for the three cases. The indoor air temperature in a clear day (case 1) is higher than in a cloudy day (cases 2 and 3). for the same day and time (July 7th at noon), we find a different thermal behaviour of the indoor air and the cooling floor, which shows the benefit of taking into account the sunshine factor in the simulations in order to have a good dimensioning.

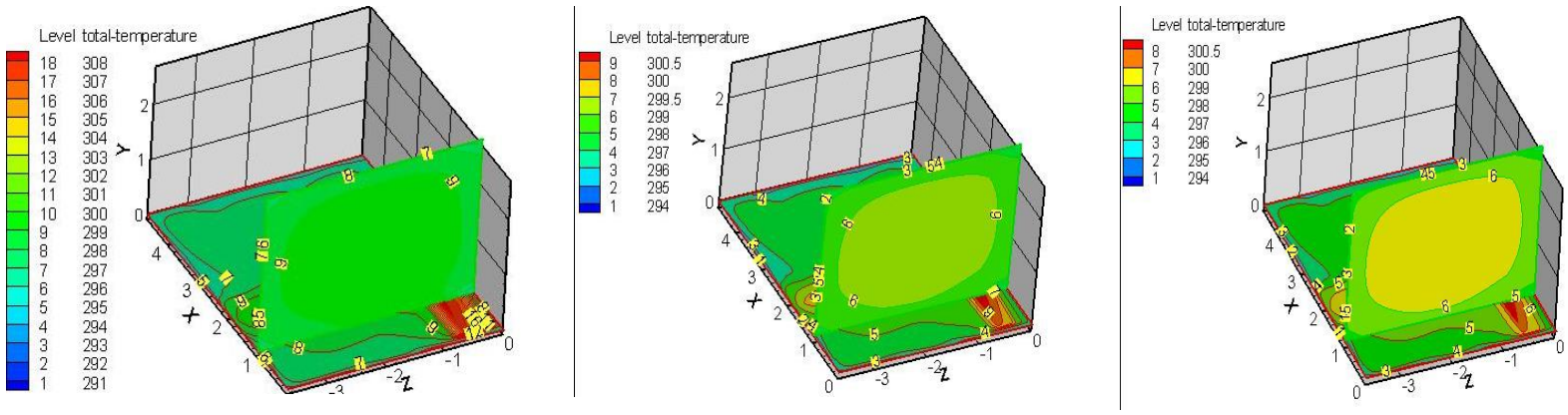

Case 1: 0% clouds **Case 2: 50% clouds** **Case 3: 80% clouds**

Figure 23: Thermal behaviour of the cooling floor and the air around the irradiated surface

6.3.4 Sunspot evolution for Bechar city

In this section we can see the evolution of the sunspot for the climatic conditions of Bechar. Bechar region is characterised by a Saharan arid and dry type climate. The purpose of this section is to show the ability the model to evaluate the sunspot effect based on the real solar power received from the region. In addition, we show the possibility of predicting other sunspot shapes. Figure 24 shows a comparison between the location (figure 24-a, b) and Surface cooling floor temperature (figure 24-c, d) for the two climates Bechar and Oran at 12 a.m on July 07. At this time, for Bechar city, we see that the sunspot shape and location on the floor are not the same as the case of Oran. These results show that the model can predict the real sunspot shape and location which depends on window geometry, location, climatic conditions and the period unlike the works cited above**.**

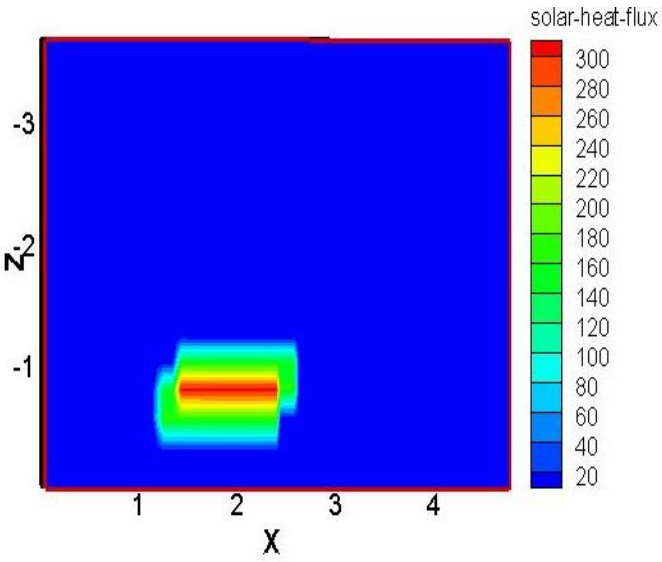

a- Sunspot location on cooling floor (Bechar city) at 12 a.m

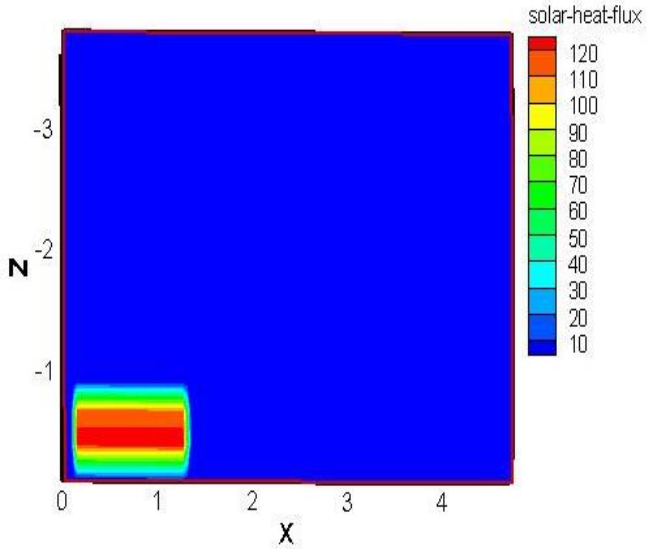

b- Sunspot location on cooling floor (Oran city) at 12 a.m

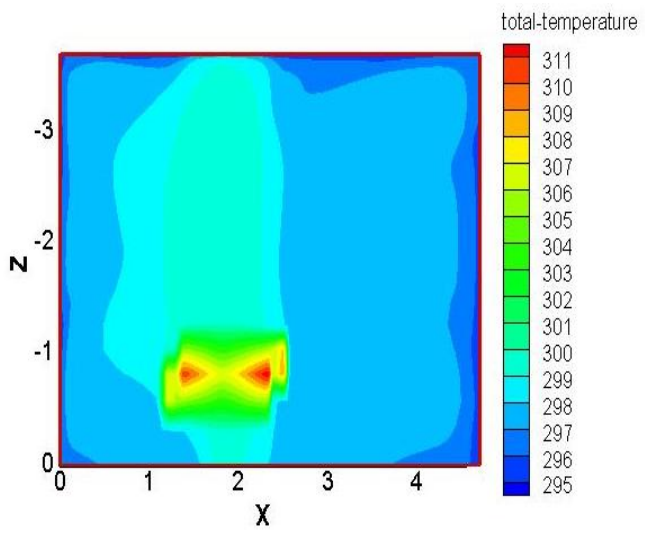

c- Surface cooling floor temperature for Bechar city at 12 a.m

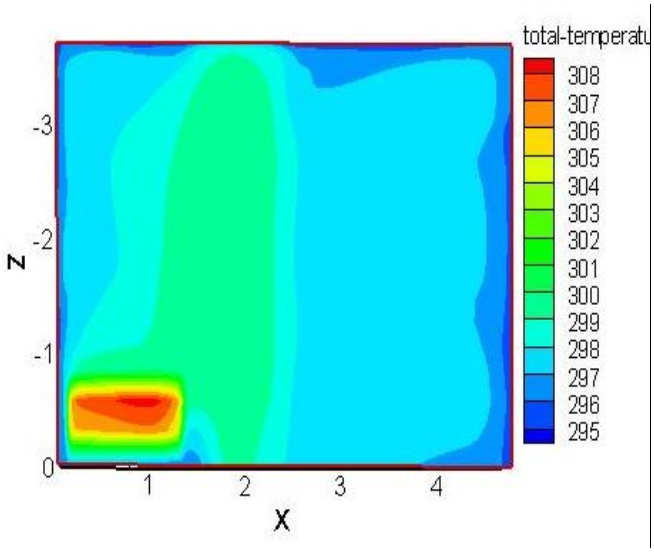

d- Surface cooling floor temperature for Oran city at 12 a.m

Figure 24: Solar heat flux (W/m^2) and surface temperature (K) of cooling floor for different climatic conditions

Figure 25 show the surface temperature and solar heat flux distributions for Bechar and Oran cities at 12 a.m. The results show that, for Bechar city, the incident solar heat flux reaches a maximum of 300 W/m^2 instead of 120 W/m^2 for Oran city. An important overheating is observed for the case of Bechar which reaches a temperature of 38°C.

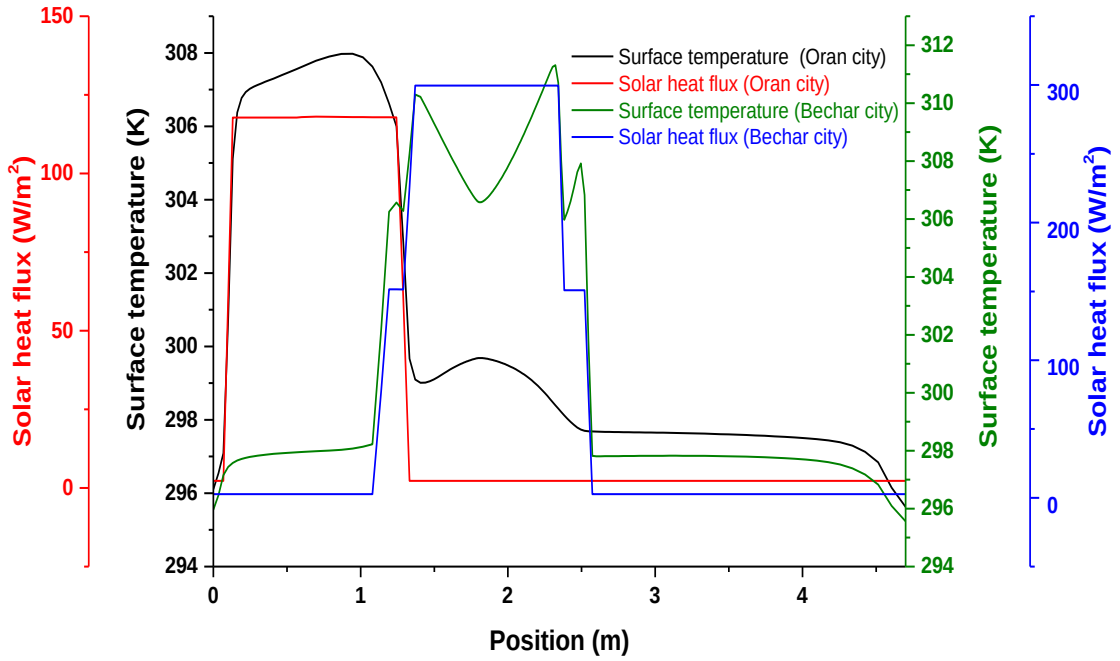

Figure 25: Surface temperature and solar heat flux on cooling floor for different climatic conditions

The absorbed and reflected solar energy on the floor don't depend only on the glazing transmissivity and floor absorptivity, but also on the outside solar radiation. The proposed model allows to quantify the reflected solar radiation in indoor air related to the weather conditions which makes it possible to predict the real behaviour of indoor air. The results of the figure 26, show that the reflected IR solar heat flux for Bechar city is 37 W/m^2 with absorptivity of 263 W/m^2. The effect of sunspot on cooling floor (Absorptivity/emissivity) in Bechar city is more important compared to Oran city with a difference of 22 W/m^2 of reflected IR solar heat flux and 158 W/m^2 of solar radiation absorbed. In this purpose, regulation system, solar protection or specific glazing is required to avoid any superheating due to the sunspot for Bechar climate.

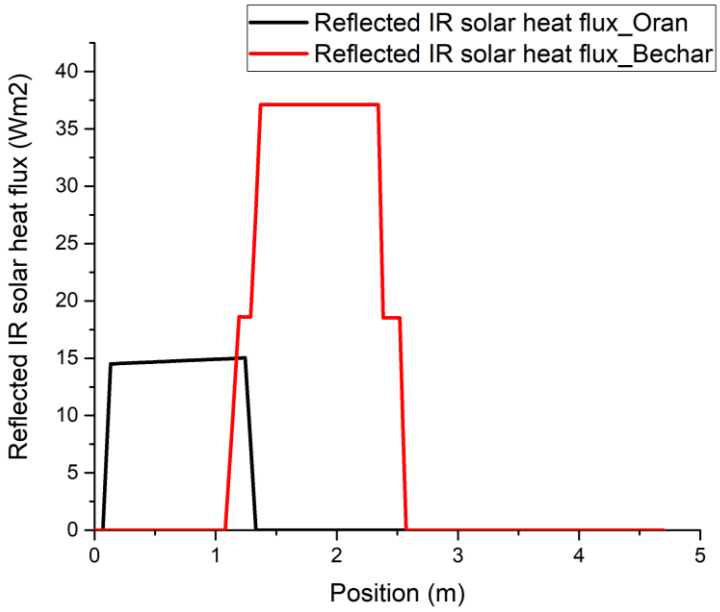

Figure 26: Reflected solar radiation for different climate

7. Study strength and limitations

In this study, we have developed a new calculation method that determines the distribution of total received solar radiation on cooling floor and it effect on indoor air in the Algerian context. Several studies have been done on sunspot effect. In this studies, the dynamic thermal behaviour of the indoor air related to the sunspot displacement and the real absorptivity/emissivity was not developed.

The strength of the study relates to the evaluation of the indoor air temperature and velocity depending on sunspot displacement. This model allows to quantify the absorbed and reflected solar power for a good dimensioning of windows and cooling floor under different climates. Therefore, we believe that our methodology can be used for other country than Algeria. More importantly, we believe that our methodology can provide the foundation for the development of thermal study and design for the Algerian context.

On the other hand, this study has limitations. The coupling between TRNSYS and FLUENT is done by a static method. We can't run continuous simulations for a long period of time. Moreover, data monitoring was done only for 10 days, and the temperature sensors were only

used for the indoor air temperature. The research could have benefited from a more extended monitoring period.

8. Implications on practice and future research

The implication of these results indicated the importance of the combination of TRNSYS and FLUENT to predict the dynamic thermal behavior of the indoor air, the received, absorbed and reflected solar radiation. We believe that building engineers can apply our findings for a good dimensioning and design of the cooling floor in the Algerian climate. We find it essential that the National Building Efficiency Standard of Algeria use our findings to improve the Algerian thermal regulation, which is under development. Hence, future works will be directed to improve this methodology taking into account a dynamic coupling for predicting a long-term effect of sunspot on existing buildings, while taking into consideration the occupant's activities.

9. Conclusion

The literature review indicates a knowledge gap that must be filled. Also, none of the published studies addressed the following issues:

- The effect of the sunspot in relation to the solar heat flux received on the cooling floor which depends on the sky state (cloudy or clear sky) and the climate conditions at different times;
- Evaluate the reflected IR solar heat flux by sunspot;
- Dynamic thermal behaviour of the indoor air of the whole room with the presence of the sunspot. This step can evaluate the thermal comfort at several levels in the room.

The present paper aims to reduce this knowledge gap and to address limitations such as (i) the study of the effect of sunspots under real meteorological conditions, (ii) the visualization of the

dynamic thermal behaviour of indoor air and surface cooling floor in relation to sunspot displacement, and (iii) the prediction of different sunspot shapes in relation to the geographical location.

Based on the results, we concluded that, presence and sunspot shifting has an effect on cooling floor temperature which causes superheating for a long period. The floor superheating can go up to 35 °C for Oran weather conditions and 38 °C for Bechar city. A wide temperature ranges of 13°C between the umbrageous and illuminated areas.

According to the ASHRAE Standing Standard Project Committee 55, spaces with passive or active systems that provide strongly non-uniform temperature and air velocity fields cause skin heat losses. The presented results show that the indoor air temperature and indoor velocity distributions are not uniform relative to the sunspot shifting that may cause discomfort. For Oran weather conditions, the indoor air temperature in the shaded area is around 24 °C, while that of the irradiated area is 28 °C for an air velocity which varies between 0.06 and 0.1 m/s.

References

[1] F. Sahnoune and K. Imessad, "Analysis and impact of the measures to mitigate climate change in Algeria," Energy Procedia, vol. 136, pp. 495–500, 2017.

[2] M.C. Lekhal, M. H. Benzaama, A. Kindinis, A. M. Mokhtari, R. Belarbi. Effect of geo-climatic conditions and pipe material on heating performance of earth-air heat exchangers. Renewable Energy 163 (2021) 22-4023.

[3] M. H. Benzaama, S. Menhoudj, K. J. Kontoleon, A. M. Mokhtari, M. C. Lekhal. Investigation of the thermal behavior of a combined geothermal system for cooling with regards to Algeria's climate, Sustainable Cities and Society 43 (2018) 121–133.

[4] S. Menhoudj, A. M. Mokhtari, M. H. Benzaama, C. Maalouf, M. Lachi, M. Makhlouf. Study of the energy performance of an Earth-Air heat exchanger for refreshing buildings in Algeria. Energy and Buildings 158 (2018) 1602–1612.

[5] M. C. Lekhal, R. Belarbi, A. M. Mokhtari, M. H. Benzaama, R. Bennacer. Thermal performance of a residential house equipped with a combined system: A direct solar floor and an earth–air heat exchanger. Sustainable Cities and Society 40 (2018) 534–545.

[6] Nasreddine Sakhri, Younes Menni, Ali J. Chamkha, Heating Capacity of an Earth to Air Heat Exchanger in Arid Regions - Experimental Investigation. Journal of Applied and Computational Mechanics. 10.22055/JACM.2020.31237.1843.

[7] Nasreddine Sakhri, Younes Menni, Ali J. Chamkha, Giulio Lorenzini, Houari Ameur, Noureddine Kaid, Mohammed Bensaf. Experimental study of an earth-to-air heat exchanger coupled to the solar chimney for heating and cooling applications in arid regions. Journal of Thermal Analysis and Calorimetry https://doi.org/10.1007/s10973-020-09867-6.

[8] Nasreddine Sakhri Younes Menni, Houari Ameur, Experimental investigation of the performance of earth-to-air heat exchangers in arid environments. Journal of Arid Environments 180 (2020) 104215.

[9] N. Sakhri, Y. Menni, H. Ameur, Effect of the pipe material and burying depthon the thermal efficiency of earth-to-air heat exchangers, Case Studies in Chemical and Environmental Engineering, https://doi.org/10.1016/j.cscee.2020.100013.

[10] Nasreddine Sakhri, Belkacem Draoui, Younes Menni, Ebrahim Elkhali Lairedj, Soufiane Merabti, Noureddine Kaid. Experimental Study of Thermal and Hygrometric Behavior of Earth to Air Heat Exchanger with Two Working Regimes in Arid Region. Proceedings of the 1st International Conference on Renewable Energy and Energy Conversion.

[11] M.-H. Benzaama, S. Menhoudj, C. Maalouf, A. Mokhtari, M. Lachi, Experimental and numerical analysis of the energy performance of a water/ soil exchanger coupled to a cooling floor for North Africa. Geothermics 80 (2019) 8–19.

[12] Benzaama, M.H., Menhoudj, S., Kontoleon, K.J., Mokhtari, A.M., Lekhal, M.C., 2018. Investigation of the thermal behavior of a combined geothermal systemfor cooling with regards to Algeria's climate. Sustainable Cities and Society 43 (2018) 121–133.

[13] X. Wu, A new simplified model to calculate surface temperature and heat transfer of radiant floor heating and cooling systems, Energy and Buildings 105 (2015) 285–293.

[14] L. Zhang, Simplified calculation for cooling/heating capacity, surface temperature distribution of radiant floor, Energy and Buildings 55 (2012) 397–404.

[15] X. Jin, Numerical simulation of radiant floor cooling system: The effects of thermal resistance of pipe and water velocity on the performance, Building and Environment 45 (2010) 2545-2552.

[16] K. Zhao, Xiao-Hua Liu, Yi Jiang Cooling capacity prediction of radiant floors in large spaces of an airpor, Solar Energy 113 (2015) 221–235.

[17] Tian, Z., Duan, B., Niu, X., Hu, Q., Niu, J., Establishment and experimental validation of a dynamic heat transfer model for concrete radiant cooling slab based on reaction coefficient method. Energy and Buildings 82 (2014) 330–340.

[18] Jingjuan (Dove) Feng, Stefano Schiavon, Fred Bauman, New method for the design of radiant floor cooling systems with solar radiation. Energy and Buildings 125 (2016) 9–18.

[19] Michele De Carli, Massimo Tonon, Effect of modelling solar radiation on the cooling performance of radiant floors. Solar Energy 85 (2011) 689–712.

[20] K. J. Kontoleon, Glazing solar heat gain analysis and optimization at varying orientations and placements in aspect of distributed radiation at the interior surfaces. Applied Energy 144 (2015) 152–164.

[21] Y. Boukhris, L. Gharbi, N.G. Morcos, Coupling the building simulation tool ZAER with a sunspot model. Case study in Tunis, Energy Build. 70 (2014) 1–14.

[22] S. Saadi, A. Chaker, M. Boubekri, Study of two new configurations of the Barra-Costantini system with sunspot modelling. Applied Thermal Engineering 173 (2020) 115221.

[23] Chihebedine Beji, Abdelatif Merabtine, Salim Mokraoui, Abdelhamid Kheiri, Julien Kauffmann, Nahla Bouaziz. Experimental study on the effects of direct sun radiation on the dynamic thermal behavior of a floor-heating system. Solar Energy 204 (2020) 1–12.

[24] Haida Tang, Tao Zhang, Xiaohua Liu, Yi Jiang, Novel method for the design of radiant floor cooling systems through homogenizing spatial solar radiation distribution. Solar Energy 170 (2018) 885–895.

[25] Athienitis A. K. and Stylianou M. (1991) Method and global relationship for estimation of transmitted solar energy distribution in passive solar rooms. Energy Sources 13, 319-336.

[26] Cucumo M., Kaliakatsos D. and Marinelli V. (1995) Estimating effective solar absorptances in rooms. Energy and Buildings 23, 117-120.

[27] Sparrow E. M. and Cess R. D. (1978) Radiation Heat Transfer, Hemisphere, Washington

[28] Rahmouni, S., Negrou, B., Settou, N., Dominguez, J., Gouareh, A. (2017). Prospects of hydrogen production potential from renewable resources in Algeria. International Journal of Hydrogen Energy, 42(2): 1383- 1395. https://doi.org/10.1016/j.ijhydene.2016.07.214.

[29]https://www.meteoblue.com/en/weather/historyclimate/climatemodelled/es-senia_algeria_2497060

[30]https://www.meteoblue.com/en/weather/historyclimate/climatemodelled/taghit_algeria_2478694

[31] B.L. Gowreesunker, S.A. Tassou, M. Kolokotroni. Coupled TRNSYS-CFD simulations evaluating the performance of PCM plate heat exchangers in an airport terminal building displacement conditioning system. Building and Environment 65 (2013) 132-145.

[32] FLUENT 6.3. Theory guide. Fluent Inc. 2006-09-20.

[33] JONAS JONSSON, Including solar load in CFD analysus of temperature distribution in a car passenger compartment. Master's thesis. Lulea University of technology.

[34]https://www.learncax.com/knowledge-base/blog/by-category/cfd/evaluate-solar-load-using-cfd

[35]https://www.padtinc.com/blog/using-the-solar-load-model-in-fluent/

[36] Qinghai Dong, Shuhong Li, Cheng Han, Numerical and experimental study of the effect of solar radiation on thermal comfort in a radiant heating system. Journal of Building Engineering 32 (2020) 101497.

[37] Bjarne Olesen. "Radiant floor cooling systems." Ashrae Journal 50.9 (2008): 16-22.

[38] American Society of Heating, Ventilating, and Air Conditioning Engineers (ASHRAE). Guideline 14-2014, Measurement of Energy and Demand Savings; Technical Report; American Society of Heating, Ventilating, and Air Conditioning Engineers: Atlanta, GA, USA, 2014.

[39] American Society of Heating, Ventilating, and Air Conditioning Engineers (ASHRAE). Guideline 14-2002, Measurement of Energy and Demand Savings; Technical Report; American Society of Heating, Ventilating, and Air Conditioning Engineers: Atlanta, GA, USA, 2002.

[40] https://en.wikipedia.org/wiki/Error_bar.